Spectrum of mesons in quenched $Sp(2N)$ gauge theories

Ed Bennett,[1,*] Jack Holligan,[2,†] Deog Ki Hong,[3,4,‡] Jong-Wan Lee,[3,4,5,§] C.-J. David Lin,[6,7,8,∥] Biagio Lucini,[9,1,¶] Maurizio Piai,[10,**] and Davide Vadacchino[11,††]

[1]*Swansea Academy of Advanced Computing, Swansea University, Fabian Way, Swansea SA1 8EN, Wales, United Kingdom*
[2]*Biomedical and Physical Sciences Building, Michigan State University, East Lansing, Michigan 48824, USA*
[3]*Department of Physics, Pusan National University, Busan 46241, Korea*
[4]*Institute for Extreme Physics, Pusan National University, Busan 46241, Korea*
[5]*Particle Theory and Cosmology Group, Center for Theoretical Physics of the Universe, Institute for Basic Science (IBS), Daejeon 34126, Korea*
[6]*Institute of Physics, National Yang Ming Chiao Tung University, 1001 Ta-Hsueh Road, Hsinchu 30010, Taiwan*
[7]*Center for High Energy Physics, Chung-Yuan Christian University, Chung-Li 32023, Taiwan*
[8]*Centre for Theoretical and Computational Physics, National Yang Ming Chiao Tung University, 1001 Ta-Hsueh Road, Hsinchu 30010, Taiwan*
[9]*Department of Mathematics, Faculty of Science and Engineering, Swansea University, Fabian Way, Swansea SA1 8EN, Wales, United Kingdom*
[10]*Department of Physics, Faculty of Science and Engineering, Swansea University, Singleton Park, Swansea SA2 8PP, Wales, United Kingdom*
[11]*Centre for Mathematical Sciences, University of Plymouth, Plymouth PL4 8AA, United Kingdom*

(Received 3 February 2024; accepted 15 April 2024; published 29 May 2024)

We report the findings of our extensive study of the spectra of flavored mesons in lattice gauge theories with symplectic gauge group and fermion matter content treated in the quenched approximation. For the $Sp(4)$, $Sp(6)$, and $Sp(8)$ gauge groups, the (Dirac) fermions transform in either the fundamental, or the 2-index, antisymmetric or symmetric, representations. This study sets the stage for future precision calculations with dynamical fermions in the low-mass region of lattice parameter space. Our results have potential phenomenological applications ranging from composite Higgs models, to top (partial) compositeness, to dark matter models with composite, strong-coupling dynamical origin. Having adopted the Wilson flow as a scale-setting procedure, we apply Wilson chiral perturbation theory to extract the continuum and massless limits for the observables of interest. The resulting measurements are used to perform a simplified extrapolation to the large-N limit, hence drawing a preliminary connection with gauge theories with unitary groups. We conclude with a brief discussion of the Weinberg sum rules.

DOI: 10.1103/PhysRevD.109.094517

I. INTRODUCTION

Strongly coupled gauge theories that live in four spacetime dimensions, have gauge group $Sp(2N)$ (for $N \in \mathbb{Z}^+$), and are coupled to fermion matter fields, have a plethora of applications in proposals of new physics that extend the Standard Model (SM) of particle physics. They can provide the microscopic origin of composite Higgs models (CHMs) [1–3],[1] and have been exploited to explain the origin of the large mass of the top quark, via the

[1]An overview of the field can be found in the review papers in Refs. [4–6], the tables in Refs. [7–9], the incomplete selection of useful papers in Refs. [10–55] and in Refs. [56–71].

*e.j.bennett@swansea.ac.uk
†holligan@msu.edu
‡dkhong@pusan.ac.kr
§j.w.lee@ibs.re.kr
∥dlin@nycu.edu.tw
¶b.lucini@swansea.ac.uk
**m.piai@swansea.ac.uk
††davide.vadacchino@plymouth.ac.uk

implementation of top partial compositeness (TPC) [72],[2] and can be used to explain for the origin of dark matter, through the strongly interacting massive particle (SIMP) paradigm [76–78],[3] and they might even affect the detectable gravitational wave (GW) stochastic background [86–91], if responsible for a phase transition in the early universe [92–97].[4]

In all these applications, the strong-coupling regime of the theory plays a central role, and hence one must develop and apply nonperturbative instruments in order to extract quantitative information about the dynamics of the theories of interest. The natural framework for such endeavor is lattice gauge theory. Until recently, the literature on $Sp(2N)$ lattice gauge theories was rather limited [116]. The discovery of the Higgs boson [117,118] has triggered a new wave of interest in extensions of the SM with strongly coupled origin, which has motivated the start of an extensive program of exploration of $Sp(2N)$ gauge theories on the lattice [119–139], as candidates for the dynamical origin of CHMs.[5]

This paper reports on new results obtained by considering $Sp(2N)$ lattice gauge theories, with $N = 2, 3, 4$, coupled to fermion matter fields treated in the quenched approximation. The effects due to fermions are not included in the Monte Carlo algorithm generating the available ensembles of configurations, but only in the formulation of the operators used to probe the underlying Yang-Mills dynamics.

There are three main, compelling motivations to perform an extended study of these theories with such approximation. Firstly, at least in the CHM and SIMP contexts, the regions of parameter space of interest for phenomenological applications are often characterized by moderately heavy fermions and sizable amounts of explicit symmetry breaking. This is needed, among other reasons, by model building consideration. In a realistic, complete model, one must ensure that the masses of towers of new composite states be large enough to have escaped direct detection so far. Furthermore, some of the new composite states must decay only via weak interactions, introduced by couplings to the SM fields. This can be achieved by making the particles heavy enough to forbid kinematically some direct decay within the strong-coupling sector. If these conditions are met, the quenched approximation may already be precise enough to produce useful estimates of the relevant spectroscopy parameters (masses and decay constants), with comparatively low investment of computing time and resources. In addition, the quenched approximation captures at once large classes of models, that differ only by the number of fermions, while the study of dynamical fermions requires dedicated Monte Carlo calculations for each choice of matter field content.

The second motivation is of a technical nature, and is closely related to the final comment we made in the previous paragraph, that already highlights both flexibility and applicability of quenched calculations. Whatever the model of interest, a systematic and rigorous dynamical study demands to benchmark it against a simpler, well understood reference example. Doing so allows to control possible systematic effects and to prevent unwanted misinterpretation of the results. It also provides a way to gauge the size of the dynamical effects due to fermions. This is particularly important, somewhat paradoxically, when studying theories for which one expects large effects to arise due to the fermion dynamics. For example, this is the case when one is looking for quasi-conformal behavior (and large anomalous dimensions) in the long distance physics of theories that are expected to be close to the boundary of the conformal window.

The third motivation for this study is that the quenched approximation, for fermions in the fundamental representation, provides a natural connection to other approaches to nonperturbative physics, in particular those relying on the large-N limit and holography [165–168]. We will not further discuss this point in the paper, but it is remarkable, for example, that the recent explosion of interest in gauge-gravity dualities has provided instruments that are particularly well suited to study the quenched, large-N limit of non-Abelian gauge theories. It is worthy of notice that the large-N limit of $Sp(2N)$ theories is expected to yield the same results, in a common sector of the physical spectrum, as the large-N_c limit for $SU(N_c)$ theories, for which the literature on lattice numerical studies is more developed—see for instance Refs. [169–172].

We study $Sp(2N)$ gauge theories with $N \geq 2$ that are asymptotically free. For the quenched fermion matter fields, we restrict attention to the three smallest possible representations: the fundamental (f), and the 2-index antisymmetric (as), and symmetric—adjoint—(s) representations. For example, the symmetry-breaking pattern of the $Sp(2N)$ theory with $N_{(\mathrm{f})} = 2$ fundamental (Dirac) fermions is described by the $SU(4)/Sp(4)$ coset relevant to minimal CHMs. With the addition of $N_{(\mathrm{as})} = 3$ (Dirac) fermions in the antisymmetric representation this theory also provides a potential microscopic realization of top partial compositeness [16]. But it is worth noting that the $N_{(\mathrm{f})} = 0$ and $N_{(\mathrm{as})} = 3$ theory is also a potential completion for a CHM [46].

[2]The reader may find it useful to refer to the more recent, critical discussions in Refs. [73–75].

[3]An incomplete list of relevant papers includes also Refs. [79–85].

[4]A number of present and future experiments might detect such effects, see for example Refs. [98–115].

[5]In parallel, extensive work on lattice gauge theories with $SU(2)$ [140–148] and $SU(4)$ [149–155] gauge groups relevant to CHMs has been performed. Lattice results on the $SU(3)$ theory with $N_f = 8$ fundamental fermions transforming in the fundamental representation [156–164] have also been used in the CHM context [47,55]—see also related earlier work in Refs. [22,23,42].

The paper is organized as follows. In Sec. II, we define the theory of interest and explain the lattice technology we deploy for this study. We present our main results for the spectra of mesons in Sec. III, organizing the material by gauge group and by representation. We briefly discuss the Weinberg sum rules, in Sec. III B. In Sec. IV, we summarize the main lessons we learned, and outline future research opportunities. The paper is supplemented by an extensive Appendix, that shows the technical details characterizing the intermediate numerical results that we analyzed to arrive at our main results.

II. LATTICE THEORY AND OBSERVABLES

In this section, we define the lattice theories of interest and the ensembles we generated, as well as the observables we computed and analyzed. We present our strategy for handling finite volume and finite spacing effects, and our scale-setting procedure. In doing so, we reorganize and consistently integrate material presented elsewhere, in particular in Refs. [119,122,124,129], but we also expand this material, and specialize it to the case of interest, as appropriate. We then describe the continuum and massless limit extrapolations, that rely on Wilson chiral perturbation theory (WχPT) [173,174] (we found it useful also to read Ref. [175], as well as some of the literature on improvement [176,177]).

A. Action and ensembles

The calculation of the mass spectrum of mesons in the quenched approximation is carried out on configurations sampled using the standard Wilson action for gauge group $Sp(2N)$:

$$S_W \equiv \beta \sum_x \sum_{\mu<\nu} \left(1 - \frac{1}{2N} \Re \mathrm{tr} P_{\mu\nu}(x)\right), \tag{1}$$

where $\beta \equiv 4N/g^2$, g is the coupling strength, $\Re$ denotes the real part and tr denotes the trace of the gauge matrix. The plaquette, $P_{\mu\nu}(x)$, is defined on the smallest closed path in the (μ,ν) plane with origin at lattice site x. A gauge link in the μ direction, originating at x, is denoted by the group element $U_\mu(x)$, hence the plaquette is

$$P_{\mu\nu}(x) = U_\mu(x) U_\nu(x + a\hat{\mu}) U_\mu^\dagger(x + a\hat{\nu}) U_\nu^\dagger(x), \tag{2}$$

with $\hat{\mu}$, $\hat{\nu}$ denoting the unit vectors in the μ, ν directions, respectively, and a the lattice spacing. We study observables for $Sp(2N)$ with $N = 2$, 3, and 4. (Later on we will present a simplified extrapolation towards asymptotically large values of N.)

The properties characterizing our ensembles are detailed in Table I, in which for each ensemble we specify N, the coupling β, the extents of the spatial, N_s, and temporal, N_t, directions of the lattice, and the gradient flow scale w_0/a—described in more detail in Sec. II C. Each meson measurement is performed from 200 lattice configurations. We use the same lattice inputs for $Sp(4)$ as in Ref. [122], to allow for direct comparison, while the choices of β are a representative subgroup of those employed in Ref. [124]—see also Ref. [129]—but we are using much larger volumes, in order to reduce finite volume effects, as discussed in Appendix A. A single update in the Markov chain consists of one application of the heat bath algorithm to each lattice link [178] and four applications of the over-relaxation algorithm [179,180]. This is defined as a single "sweep". We perform an initial 600 sweeps to thermalize the lattice and thereafter apply 12 sweeps between each of the 200 configurations, to reduce autocorrelation. We checked that none of the ensembles used for this analysis show significant evidence of topological freezing.

TABLE I. Lattice ensembles analyzed in the Yang-Mills $Sp(2N)$ gauge theories of interest. We report the value of N, of the lattice coupling, β, of the spatial, N_s, and temporal, N_t, extension of the lattice, as well as the gradient flow scale, w_0, expressed in units of the lattice spacing, a.

N	β	$N_s^3 \times N_t$	w_0/a
2	7.62	$24^3 \times 48$	1.31800(95)
	7.7	$48^3 \times 60$	1.45284(40)
	7.85	$48^3 \times 60$	1.76364(63)
	8.0	$48^3 \times 60$	2.10735(99)
	8.2	$48^3 \times 60$	2.6188(23)
3	15.6	$24^3 \times 48$	1.29831(67)
	16.1	$24^3 \times 48$	1.8000(17)
	16.5	$48^3 \times 96$	2.24078(99)
	16.7	$48^3 \times 96$	2.5040(11)
	17.1	$48^3 \times 96$	3.0768(24)
4	26.5	$24^3 \times 48$	1.34724(48)
	26.7	$48^3 \times 96$	1.44654(17)
	26.8	$48^3 \times 96$	1.50491(17)
	27.0	$48^3 \times 96$	1.62325(25)
	27.3	$60^3 \times 120$	1.80187(25)

B. Mesons

The observable quantities of interest for this paper are the flavor nonsinglet meson masses and the related decay constants. They are measured by examining the large-time behavior of two-point correlation functions involving interpolating operators sourcing the mesons, which we denote as $\mathcal{O}_M$. We list the interesting operators and their properties in Table II.

Masses and decay constants of mesons made of fermions transforming in the fundamental representation in a channel labelled as M are denoted as m_M and f_M, respectively. Because we study mesons comprised of fermions transforming in three distinct representations of the group, in order to distinguish them we change the aspect of the label.

TABLE II. Interpolating operators, $\mathcal{O}_M$, appearing in the correlation functions computed for this publication. For each operator, we indicate their name, label, Dirac algebra structure, spin, J, and parity, P, of the associated mesons. We find it convenient to also associate each operator with the meson sourced by the analogous QCD operator.

Channel	Label	$\mathcal{O}_M$	J^P	QCD meson
Pseudoscalar	PS	$\bar{\psi}\gamma_5\psi$	0^-	π
Scalar	S	$\bar{\psi}\psi$	0^+	a_0
Vector	V	$\bar{\psi}\gamma_\mu\psi$	1^-	ρ
Axial-vector	AV	$\bar{\psi}\gamma_5\gamma_\mu\psi$	1^+	a_1
Tensor	T	$\bar{\psi}\gamma_0\gamma_\mu\psi$	1^-	ρ
Axial-tensor	AT	$\bar{\psi}\gamma_5\gamma_0\gamma_\mu\psi$	1^+	b_1

While retaining upper case labels for the (f) fermions, mesons made of (as) fermions have lower case labels, and calligraphic lettters are used for the labels of mesons made of (s) fermions. For example, the pseudoscalar masses in the (f), (as), and (s) cases are denoted by $m_{\rm PS}$, $m_{\rm ps}$, and $m_{\mathcal{PS}}$, respectively. In Table II and in rest of this subsection, we denote a general channel by an uppercase, e.g., as M, to lighten the notation, the replacements needed for the other two cases being clear from the context.

The zero-momentum 2-point correlation function of operators $\mathcal{O}_M$ and $\mathcal{O}_{M'}$ is defined as

$$C_{M,M'}(t) \equiv \sum_{\vec{x}} \langle 0|\mathcal{O}_M(\vec{x},t)\mathcal{O}^\dagger_{M'}(\vec{0},0)|0\rangle. \qquad (3)$$

We set $M = M'$, and examine the large-time behavior of the correlation function, that we approximate as follows:

$$C_{M,M}(t\to\infty) \simeq \frac{|\langle 0|\mathcal{O}_M|M\rangle|^2}{2m_M}(e^{-m_M t} + e^{-m_M(T-t)}), \qquad (4)$$

having ignored contamination from states other than the lightest one. In the case of S, T and AT channels, we measure only the mass of the ground state composite particle. In the other three cases (PS, V and AV), we extract also the decay constant, besides the mass. To do so, for V and AV channels we exploit the fact that the matrix elements obey the following relations:

$$\langle 0|\mathcal{O}^\mu_{\rm V}|{\rm V}\rangle = f_{\rm V} m_{\rm V}\epsilon^\mu, \qquad (5)$$

$$\langle 0|\mathcal{O}^\mu_{\rm AV}|{\rm AV}\rangle = f_{\rm AV} m_{\rm AV}\epsilon^\mu, \qquad (6)$$

where ϵ^μ is the polarization vector, normalized so that $\epsilon^\mu\epsilon_\mu = 1$.

For the decay constant of the pseudoscalar mesons, we use one additional correlation function:

$$C_{\rm AV,PS}(t) = \sum_{\vec{x}} \langle 0|\mathcal{O}_{\rm AV}(\vec{x},t)\mathcal{O}^\dagger_{\rm PS}(\vec{0},0)|0\rangle. \qquad (7)$$

Its large-time behavior is expected to be described as

$$C_{\rm AV,PS}(t\to\infty) \simeq \frac{f_{\rm PS}\langle 0|\mathcal{O}_{PS}|PS\rangle^*}{2m_{PS}}(e^{-m_{PS}t} - e^{-m_{\rm PS}(T-t)}). \qquad (8)$$

The normalizations are chosen so that the corresponding decay constant in QCD is $f_\pi \simeq 93$ MeV.

From the large-time behavior of all these correlation functions, we can hence measure nine observables, for each of the three types of fermions, and for each of the three gauge groups.

C. Scale setting

We adopt a scale-setting procedure that is especially suited to studies of novel strongly coupled models, and is based on the gradient flow and its lattice implementation, the Wilson flow [181,182]. We follow the same process outlined in Ref. [129], in the context of the $Sp(2N)$ lattice program, and report here only basic definitions necessary to fix the notation in the following.

The gradient flow for gauge fields, $B_\mu(\mathbb{t},x)$, is defined by solving in five space-time dimensions the differential equation,

$$\frac{{\rm d}B_\mu(\mathbb{t},x)}{{\rm d}\mathbb{t}} = D_\nu F_{\mu\nu}(\mathbb{t},x), \qquad B_\mu(0,x) = A_\mu(x), \qquad (9)$$

where $\mathbb{t}$ is known as flow-time, $D_\mu \equiv \partial_\mu + [B_\mu,\cdot]$ and $F_{\mu\nu}(\mathbb{t},x) \equiv [D_\mu, D_\nu]$. The flow defined by the above equation drives the configuration $A_\mu(x)$ at $\mathbb{t} = 0$ of the gauge fields towards a stationary point of the continuum Yang-Mills action. It is possible to show that, at leading order in the gauge coupling, it implements a Gaussian smoothening of the field over a region of mean-square radius $\sqrt{8\mathbb{t}}$. A renormalized coupling, α, can then be defined at this scale as follows:

$$\alpha(\mu^{-1} = \sqrt{8\mathbb{t}}) \equiv k_\alpha \mathbb{t}^2\langle E(\mathbb{t})\rangle \equiv k_\alpha \mathcal{E}(\mathbb{t}), \qquad (10)$$

where $E(\mathbb{t}) = \frac{1}{4}F_{\mu\nu}(\mathbb{t})F^{\mu\nu}(\mathbb{t})$, and k_α is a numerical coefficient that can be extracted from perturbation theory [183]. A reference scale $\mathbb{t}_0$ can be defined implicitly as follows:

$$\mathcal{E}(\mathbb{t}_0) = \mathbb{t}^2\langle E(\mathbb{t})\rangle|_{\mathbb{t}=\mathbb{t}_0} = \mathcal{E}_0, \qquad (11)$$

with a conventional choice of $\mathcal{E}_0$. Alternatively, one can define the related quantity

$$\mathcal{W}(\mathbb{t}) = \mathbb{t}\frac{\rm d}{{\rm d}\mathbb{t}}\mathcal{E}(\mathbb{t}), \qquad (12)$$

and the scale w_0 as

$$\mathcal{W}(\mathbb{t} = w_0^2) = \mathcal{W}_0, \tag{13}$$

for an appropriate, conventional choice of $\mathcal{W}_0$ [184].

On the lattice, the *Wilson* flow $V_\mu(\mathbb{t})$ is defined by solving the differential system:

$$\frac{\mathrm{d}V_\mu(\mathbb{t},x)}{\mathrm{d}\mathbb{t}} = -g_0^2(\partial_{x,\mu}S^{\mathrm{flow}}[V_\mu])V(\mathbb{t},x), \tag{14}$$

$$V_\mu(0,x) = U_\mu(x), \tag{15}$$

where $S^{\mathrm{flow}}[V_\mu]$ is the Wilson action. The configurations $U_\mu(x)$ in a given ensemble are used as initial conditions for the system, and the flow is obtained by numerical integration. The lattice observables are then computed with the resulting, finite flow-time, smoothened configurations. In order to compute the Wilson flow scale, w_0, on the lattice, we adopted the clover-leaf discretization for $E(\mathbb{t})$. We follow the strategy described in detail in Ref. [129] in order to fix reference values for $\mathcal{W}_0$ for different choices of N. We summarize in Table I the resulting value of $1/\hat{a} \equiv w_0/a$ thus obtained. In the following, we adopt the hatted notation to present dimensional quantities in units of the gradient flow scale, i.e., $\hat{m} = mw_0$, for a generic mass m.

D. Continuum and massless extrapolation

As we discussed in the introduction to this paper, the quenched approximation is expected to yield reasonably good estimates for observable quantities when the fermion contribution to the dynamics is small. This is the case for moderately large fermion masses, but also when the number of (f)-type fermions is small while the number of colors is large. We extrapolate our numerical lattice data to the continuum and massless limit simultaneously. As we look at comparatively large groups, such as $Sp(8)$, it is also interesting to perform extrapolations to the large-N limit as well. Yet, before proceeding to describe our analysis, we alert the reader to use some caution when using the results of such extrapolations in phenomenological applications, in view of the systematic uncertainty intrinsic in the quenched approximation.

Having set the scale using the Wilson flow, we follow a procedure inspired by WχPT prescription [173,174], truncated at the next-to-leading order; see also Refs. [121,122] for earlier implementations of this strategy in $Sp(2N)$ theories. The same formal expression holds for masses and decay constants:

$$\hat{m}_{\mathrm{M}}^{2,\mathrm{NLO}} = \hat{m}_{\mathrm{M}}^{2,\chi}(1 + L_{m,\mathrm{M}}^0\hat{m}_{\mathrm{PS}}^2) + W_{m,\mathrm{M}}^0\hat{a}, \tag{16}$$

$$\hat{f}_{\mathrm{M}}^{2,\mathrm{NLO}} = \hat{f}_{\mathrm{M}}^{2,\chi}(1 + L_{f,\mathrm{M}}^0\hat{m}_{\mathrm{PS}}^2) + W_{f,\mathrm{M}}^0\hat{a}, \tag{17}$$

where the superscript χ denotes a quantity in the massless limit, with $1/\hat{a} \equiv w_0/a$, and $\hat{m}_{\mathrm{PS}}$ the mass of pseudoscalar meson in units of the gradient flow scale [in the appropriate representation of $Sp(2N)$]. The coefficients appearing on the right-hand side of these relations are extracted by fitting numerical results obtained with different values of lattice coupling, β, and fermion masses.

III. SUMMARY OF RESULTS

In this section, we display, summarize, and critically discuss our final results, extrapolated to the massless and continuum limits. Details about the intermediate results can be found in the Appendix, and in the data release [185]. Given the correlator, $C(t)$, we can extract the effective mass accounting for both forward- and backward-propagations in Euclidean time, t, defining the effective mass as

$$m_{\mathrm{eff}}(t) = \mathrm{arccosh}\left[\frac{C(t+a) + C(t-a)}{2C(t)}\right]. \tag{18}$$

We include in the analysis only numerical results obtained from ensembles for which we found unambiguous evidence of a clear plateau in the effective-mass plot.

We restricted attention to cases in which finite-volume effects are smaller than the statistical uncertainties; see Appendix A and Fig. 4. Our results for the continuum, massless extrapolations are listed in Tables III–V. The masses and decay constants of mesons made of (quenched) fermions of type (f), (as), and (s), respectively, are displayed in Figs. 1–3. All these plots show the 1σ-equivalent best-fit ranges, obtained by bootstrapping the statistical error through the maximum likelihood process based upon WχPT. We report the mass of the lowest excitation in the V, AV, S, T, and AT channels, and the decay constants of the PS, V, and AV lightest states, omitting few cases in which the measurements are inconclusive.

Before discussing the individual results, we highlight the presence of five major sources of systematic effects in this study. First and foremost, the calculations use quenched fermions, hence part of the dynamics is not included faithfully in the Monte Carlo process generating the ensembles. One expects the results to be reasonably accurate in the limit in which the number of fermions is small, or their mass is large. Available measurements for the $Sp(4)$ theory with $N_{(\mathrm{f})} = 2$ fermions transforming in the fundamental representation suggest that the discrepancy might not exceed the level of $10\% \div 25\%$, but this conclusion depends on the observable of interest [121]. In order to achieve a better precision, particularly to include large number of fermions—for example, by approaching the lower end of the conformal window—dedicated calculations with dynamical fermions are needed.

In the numerical calculations the fermion mass is large enough to kinematically prevent the lightest V meson decay

TABLE III. Massless and continuum extrapolation of the decay constants, $\hat{f}$, and masses, $\hat{m}$, expressed in units of the gradient flow scale, w_0, for quenched mesons in the $Sp(4)$ theory, for the three representations considered in this study. The uncertainties reported are determined by the extrapolation, starting from the statistical uncertainties of the individual measurements. Reduced chi-squared values, $\chi^2/N_{\mathrm{d.o.f.}}$, that are greater than 3.0 are highlighted in bold (e.g., 3.06). All $Sp(4)$ measurements with (f) or (as) mesons have been performed on newly generated configurations, and agree, within errors, with those reported in Ref. [122]. The massless and continuum extrapolations for $\hat{f}^2_{\mathrm{AV}}$ and $\hat{f}^2_{\mathrm{av}}$, which are displayed by the plots in Appendix B, are affected by large systematics due to numerical noise.

	$Sp(4)$		
Representation	Channel	Chiral limit	χ^2/d.o.f.
Fundamental	$\hat{f}_{\mathrm{PS}}$	0.0818(11)	1.30
	$\hat{f}_{\mathrm{V}}$	0.1603(29)	1.60
	$\hat{f}_{\mathrm{AV}}$	0.215(12)	1.10
	$\hat{m}_{\mathrm{V}}$	0.6022(49)	1.63
	$\hat{m}_{\mathrm{AV}}$	1.087(43)	1.04
	$\hat{m}_{\mathrm{S}}$	1.052(38)	2.97
	$\hat{m}_{\mathrm{T}}$	0.5991(81)	1.47
	$\hat{m}_{\mathrm{AT}}$	1.145(48)	2.21
Antisymmetric	$\hat{f}_{\mathrm{ps}}$	0.1084(12)	1.06
	$\hat{f}_{\mathrm{v}}$	0.1917(66)	1.37
	$\hat{f}_{\mathrm{av}}$	0.254(17)	1.67
	$\hat{m}_{\mathrm{v}}$	0.7459(90)	1.21
	$\hat{m}_{\mathrm{av}}$	1.270(63)	1.33
	$\hat{m}_{\mathrm{s}}$	1.129(65)	1.71
	$\hat{m}_{\mathrm{t}}$	0.774(14)	1.95
	$\hat{m}_{\mathrm{at}}$	1.408(75)	1.97
Symmetric	$\hat{f}_{\mathcal{PS}}$	0.1535(19)	2.42
	$\hat{f}_{\mathcal{V}}$	0.276(12)	1.56
	$\hat{f}_{\mathcal{AV}}$	0.406(20)	2.47
	$\hat{m}_{\mathcal{V}}$	0.881(11)	1.29
	$\hat{m}_{\mathcal{AV}}$	1.460(71)	2.07
	$\hat{m}_{\mathcal{S}}$	1.284(54)	**3.06**
	$\hat{m}_{\mathcal{T}}$	0.902(16)	**3.07**
	$\hat{m}_{\mathcal{AT}}$	2.077(99)	**3.38**

TABLE IV. Massless and continuum extrapolation of the decay constants, $\hat{f}$, and masses, $\hat{m}$, expressed in units of the gradient flow scale, w_0, for quenched mesons in the $Sp(6)$ theory, for the three representations considered in this study. The uncertainties reported are determined by the extrapolation, starting from the statistical uncertainties of the individual measurements.

	$Sp(6)$		
Representation	Channel	Chiral limit	χ^2/d.o.f.
Fundamental	$\hat{f}_{\mathrm{PS}}$	0.1073(20)	1.56
	$\hat{f}_{\mathrm{V}}$	0.1922(67)	1.84
	$\hat{f}_{\mathrm{AV}}$	0.235(17)	1.78
	$\hat{m}_{\mathrm{V}}$	0.5890(86)	1.71
	$\hat{m}_{\mathrm{AV}}$	1.062(55)	1.59
	$\hat{m}_{\mathrm{S}}$	0.846(64)	1.38
	$\hat{m}_{\mathrm{T}}$	0.610(13)	1.11
	$\hat{m}_{\mathrm{AT}}$	1.090(68)	2.06
Antisymmetric	$\hat{f}_{\mathrm{ps}}$	0.1940(32)	2.89
	$\hat{f}_{\mathrm{v}}$	0.353(18)	1.90
	$\hat{f}_{\mathrm{av}}$	0.267(24)	1.26
	$\hat{m}_{\mathrm{v}}$	0.782(12)	1.47
	$\hat{m}_{\mathrm{av}}$	1.026(83)	1.13
	$\hat{m}_{\mathrm{s}}$	0.897(68)	1.00
	$\hat{m}_{\mathrm{t}}$	0.779(19)	1.24
	$\hat{m}_{\mathrm{at}}$	1.468(94)	1.67
Symmetric	$\hat{f}_{\mathcal{PS}}$	0.2142(51)	2.72
	$\hat{f}_{\mathcal{V}}$	0.476(19)	2.28
	$\hat{f}_{\mathcal{AV}}$	0.426(39)	1.97
	$\hat{m}_{\mathcal{V}}$	0.912(10)	1.56
	$\hat{m}_{\mathcal{AV}}$	1.027(93)	1.42
	$\hat{m}_{\mathcal{S}}$	0.673(62)	0.59
	$\hat{m}_{\mathcal{T}}$	0.893(19)	2.08
	$\hat{m}_{\mathcal{AT}}$	1.61(14)	1.07

to PS pairs. On theoretical grounds, we know that the quenched approximation may lead to unitarity problems in the low-mass region, and hence we avoid it. Empirically, we also found that finite-volume effects become severe when we use light masses in the fermion propagators, hence we restricted attention to choices for which $m_{\mathrm{PS}}/m_{\mathrm{V}} \gtrsim 0.6$. The reader should hence exercise some caution in using the results of next-to-leading-order WχPT to extrapolate to massless and continuum limits.

A third limitation is given by the fact that some of the meson masses are comparatively large, when expressed in lattice units. We retained in the analysis only ensembles and choices of the fermion masses for which $m_{\mathrm{PS}}a \ll 1$, but the masses of the AV, AT, and S states are often far larger. This lattice artifact manifests itself as a deterioration of the signal in the effective mass plots, particularly in the S and AT channels for the (as) and (s) fermions.

One way to ameliorate the aforementioned difficulty would be to perform the study on finer lattices, hence raising the intrinsic cutoff of the theory and reducing finite-spacing effects. To do so would require the adoption of larger values of the lattice coupling, β. Unfortunately, by doing so autocorrelation grows, thermalization takes longer, and the calculations would become too expensive to justify within the quenched approximation. Furthermore, this might lead to topological freezing, especially for large groups, $Sp(6)$ and $Sp(8)$.

A simple way of visualizing the size of finite-spacing effects is to display the measurements of masses and decay constants of the mesons at finite β, together with their extrapolations obtained with WχPT. We report in the Appendix a catalog of such plots. The extrapolations for

TABLE V. Massless and continuum extrapolation of the decay constants, $\hat{f}$, and masses, $\hat{m}$, expressed in units of the gradient flow scale, w_0, for quenched mesons in the $Sp(8)$ theory, for the three representations considered in this study. The uncertainties reported are determined by the extrapolation, starting from the statistical uncertainties of the individual measurements. Reduced chi-squared values, $\chi^2/N_{\mathrm{d.o.f.}}$, that are greater than 3.0 are highlighted in bold (e.g., 3.02).

$Sp(8)$			
Representation	Channel	Chiral limit	χ^2/d.o.f.
Fundamental	$\hat{f}_{\mathrm{PS}}$	0.1117(20)	0.48
	$\hat{f}_{\mathrm{V}}$	0.1921(80)	0.68
	$\hat{f}_{\mathrm{AV}}$	0.245(19)	1.69
	$\hat{m}_{\mathrm{V}}$	0.5782(66)	0.74
	$\hat{m}_{\mathrm{AV}}$	0.993(56)	1.38
	$\hat{m}_{\mathrm{S}}$	0.856(52)	0.72
	$\hat{m}_{\mathrm{T}}$	0.573(11)	1.23
	$\hat{m}_{\mathrm{AT}}$	0.963(65)	0.82
Antisymmetric	$\hat{f}_{\mathrm{ps}}$	0.2152(43)	1.85
	$\hat{f}_{\mathrm{v}}$	0.434(19)	1.20
	$\hat{f}_{\mathrm{av}}$	…	…
	$\hat{m}_{\mathrm{v}}$	0.7955(63)	1.23
	$\hat{m}_{\mathrm{av}}$	…	…
	$\hat{m}_{\mathrm{s}}$	…	…
	$\hat{m}_{\mathrm{t}}$	0.8085(88)	0.94
	$\hat{m}_{\mathrm{at}}$	…	…
Symmetric	$\hat{f}_{\mathcal{PS}}$	0.2380(64)	1.80
	$\hat{f}_{\mathcal{V}}$	0.677(15)	1.63
	$\hat{f}_{\mathcal{AV}}$	…	…
	$\hat{m}_{\mathcal{V}}$	0.9513(53)	**3.02**
	$\hat{m}_{\mathcal{AV}}$	…	…
	$\hat{m}_{\mathcal{S}}$	…	…
	$\hat{m}_{\mathcal{T}}$	0.9608(72)	1.81
	$\hat{m}_{\mathcal{AT}}$	…	…

the mass of the V and T states are affected by rather large finite-spacing effects. For the purpose of this paper, of benchmarking the space of $Sp(2N)$ theories coupled to matter fermion fields, this is adequate. Future precision studies with dynamical fermions will require a more radical approach, possibly involving improving the action.

Finally, we conducted a quite extensive study of the size of finite-volume effects (see Appendix A, as well as the example in Fig. 4). Given the comparative simplicity of the dynamics implemented in the ensemble generation, we could generate many ensembles, by varying the volume up to $\tilde{V} = 60^3 \times 120 \times a^4$, hence ensuring that this source of systematic effects can be completely ignored. Interestingly, we found that for finite volume effects to be smaller than statistical uncertainties we must use volumes for which $m_{\mathrm{PS}}L \gtrsim 8$ for $Sp(6)$ (as shown in Fig. 4), or even $m_{\mathrm{PS}}L \gtrsim 11$ for $Sp(8)$. This finding highlights the need to perform dedicated studies of finite volume effects in calculations with dynamical fermions, as such strong requirements might prove computationally challenging to meet.[6]

Having discussed the main sources of systematic uncertainty, we can now proceed to comment on our results for the physical observables, starting from the case of matter transforming in the fundamental representation. The top panel of Fig. 1 shows that the lightest state is a V meson, corresponding to the ρ meson in QCD. The degeneracy between V and T channels agrees with current algebra, within the uncertainties, for all $Sp(N_c = 2N)$ theories considered here. All states in AV, AT and S channels are heavier, and affected by sizable errors. Their masses, expressed in units of w_0, tend consistently to decrease with N_c, but appear to converge to a finite result. Conversely, the decay constants squared (bottom panel of Fig. 1) grow proportionally to N_c, as expected from large-N_c arguments. Even after taking into account their leading-order N_c behavior, we find residual dependence on N_c, as discussed in the following subsection. Figures 2 and 3 display the same information, but for mesons made of (as) and (a) fermions. Again, the vector and tensor states are the lightest, and degenerate, as expected. The decay constant for mesons made of matter transforming in the 2-index representations scale with N_c^2.

A. Towards large N

Figures 1–3 display also the result of extrapolating the numerical results to the large-N_c limit. This is performed by assuming that all the squares of the meson masses exhibit the following behavior:

$$\hat{m}_M^2(N_c) = \hat{m}_M^2(\infty) + \frac{\Delta \hat{m}_M^2(\infty)}{N_c}. \tag{19}$$

In the case of the square of the decay constants, we assume the following relations to hold:

$$\frac{\hat{f}_M^2(N_c)}{N_c} = \frac{\hat{f}_M^2(\infty)}{N_c} + \frac{\Delta \hat{f}_M^2(\infty)}{N_c^2}, \tag{20}$$

$$\frac{\hat{f}_m^2(N_c)}{N_c^2} = \frac{\hat{f}_m^2(\infty)}{N_c^2} + \frac{\Delta \hat{f}_m^2(\infty)}{N_c^3}, \tag{21}$$

$$\frac{\hat{f}_{\mathcal{M}}^2(N_c)}{N_c^2} = \frac{\hat{f}_{\mathcal{M}}^2(\infty)}{N_c^2} + \frac{\Delta \hat{f}_{\mathcal{M}}^2(\infty)}{N_c^3}, \tag{22}$$

for mesons constituted of (f), (as), and (s) fermions, respectively. As (in most cases) three independent measurements are available, obtained for $Sp(4)$, $Sp(6)$, and $Sp(8)$, we apply a maximum likelihood analysis to extract

[6]Note that finite volume effects can be more severe in the quenched approximation, see Refs. [186,187].

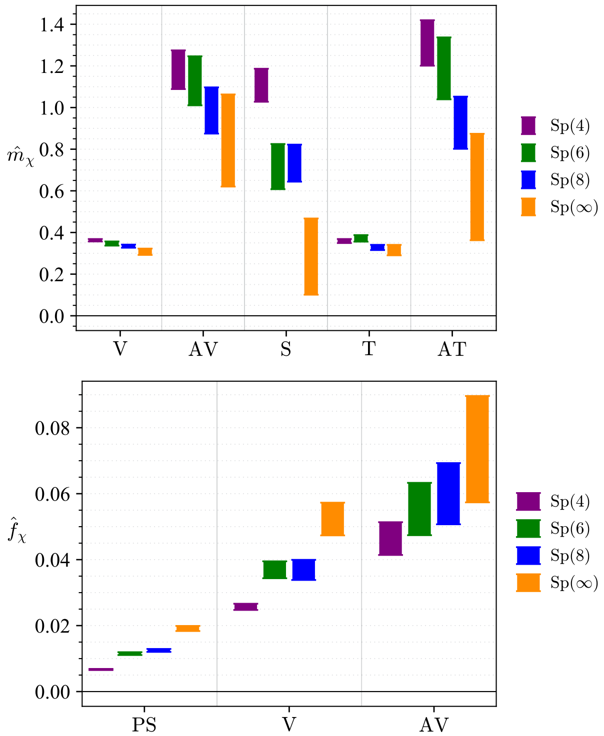

FIG. 1. Masses (top) and decay constants (bottom) squared of mesons in the $Sp(N_c)$ theory with (quenched) matter consisting of fermions transforming in the fundamental representation, (f), extrapolated to the massless and continuum limits, expressed in units of the gradient flow scale, w_0, computed for $N_c = 4$, 6, 8, and further extrapolated to $N_c \to \infty$.

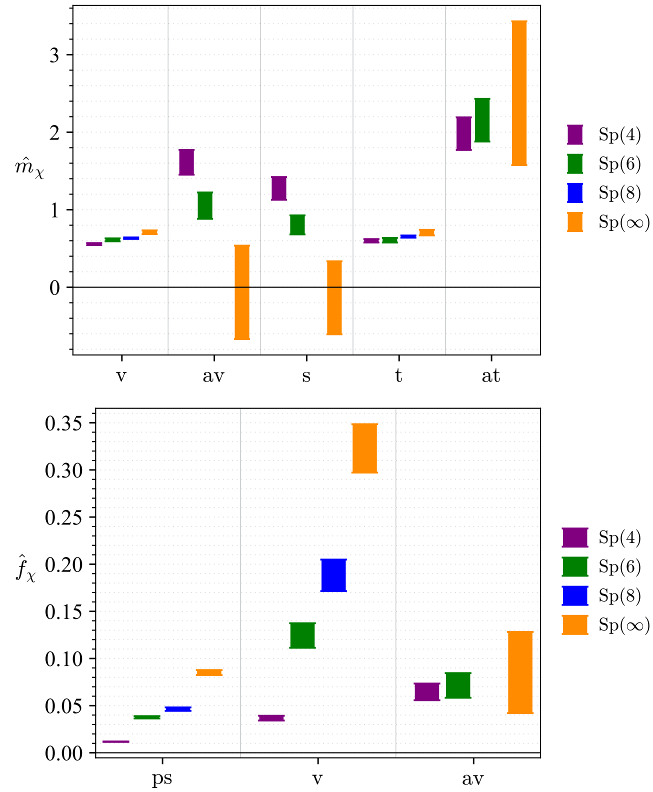

FIG. 2. Masses (top) and decay constants (bottom) squared of mesons in the $Sp(N_c)$ theory with (quenched) matter consisting of fermions transforming in the 2-index antisymmetric representation, (as), extrapolated to the massless and continuum limits, expressed in units of the gradient flow scale, w_0, computed for $N_c = 4$, 6, 8, and further extrapolated to $N_c \to \infty$.

the two unknown coefficients, and perform the $N_c \to +\infty$ extrapolations.

In the case of fermions transforming on the antisymmetric and symmetric representations, mesons and decay constants tend to be larger than in the fundamental case, but are affected by bigger uncertainties. We can still verify that the lightest states in the V and T channel are degenerate, as expected, but in several examples we are not able to measure the mass and decay constant for the $Sp(8)$ case, as shown in Table V. In such occurrences, the large-N_c limit is obtained by simple extrapolation from the two available data points (see Table VI).

We do not find agreement in the large-N extrapolations of the properties of mesons made of (as) and (s) fermions, with the noticeable exception of the decay constant of the pseudoscalar state. This fact, combined with the large value of some $\chi^2/N_{\mathrm{d.o.f}}$, and with the fact that for many observables we could not use $Sp(8)$ results, suggests that the large-N extrapolations for the mesons made of (s) fermions are affected by large systematic uncertainties, and should not be used in phenomenological studies. We decided to report these results, despite their poor quality, to illustrate the fact that, in order to study the large-N limit of this type of mesons, a more refined numerical strategy will be needed. We remind the reader that our main objective in this paper is to benchmark what is achievable within this large class of theories, hence even such negative result is of some value. Similar conservative arguments may apply also to the $Sp(8)$ theory with (as) fermions, while for $Sp(4)$ and $Sp(6)$ the measurements performed with (as) fermions yield reasonable results, and the values of $\chi^2/N_{\mathrm{d.o.f}}$ are acceptable.

B. Sum rules

The Weinberg sum rules [189] are exact results, that can be formulated as follows:

$$\sum_i (\hat{f}^2_{\mathrm{V},i} - \hat{f}^2_{\mathrm{AV},i}) = \hat{f}^2_{\mathrm{PS}}, \tag{23}$$

$$\sum_i (\hat{m}^2_{\mathrm{V},i}\hat{f}^2_{\mathrm{V},i} - \hat{m}^2_{\mathrm{AV},i}\hat{f}^2_{\mathrm{AV},i}) = 0, \tag{24}$$

where the summation is over the whole tower of states sourced by the V and AV meson operators. It is interesting to question whether these rules can be saturated by

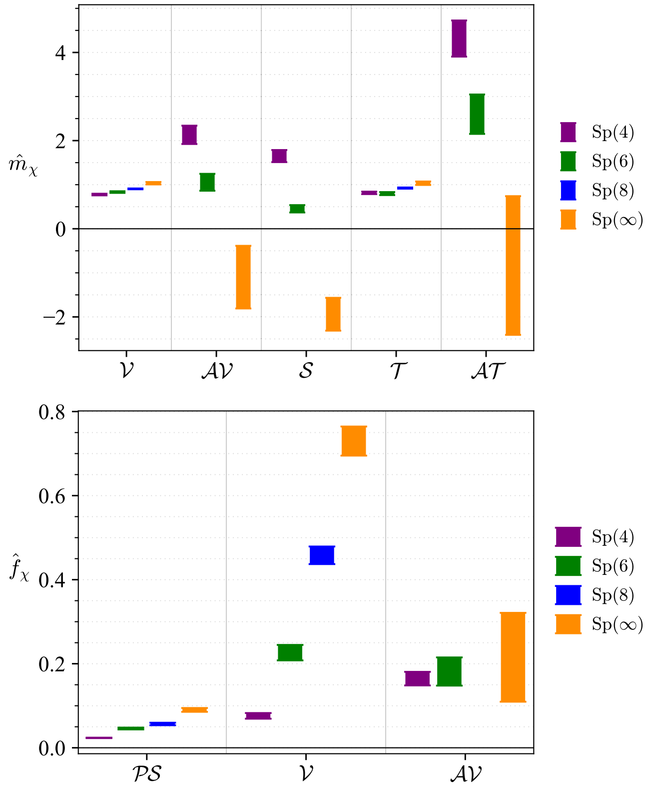

FIG. 3. Masses (top) and decay constants (bottom) squared of mesons in the $Sp(N_c)$ theory with (quenched) matter consisting of fermions transforming in the 2-index symmetric representation, (s), extrapolated to the massless and continuum limits, expressed in units of the gradient flow scale, w_0, computed for $N_c = 4$, 6, 8, and further extrapolated to $N_c \to \infty$.

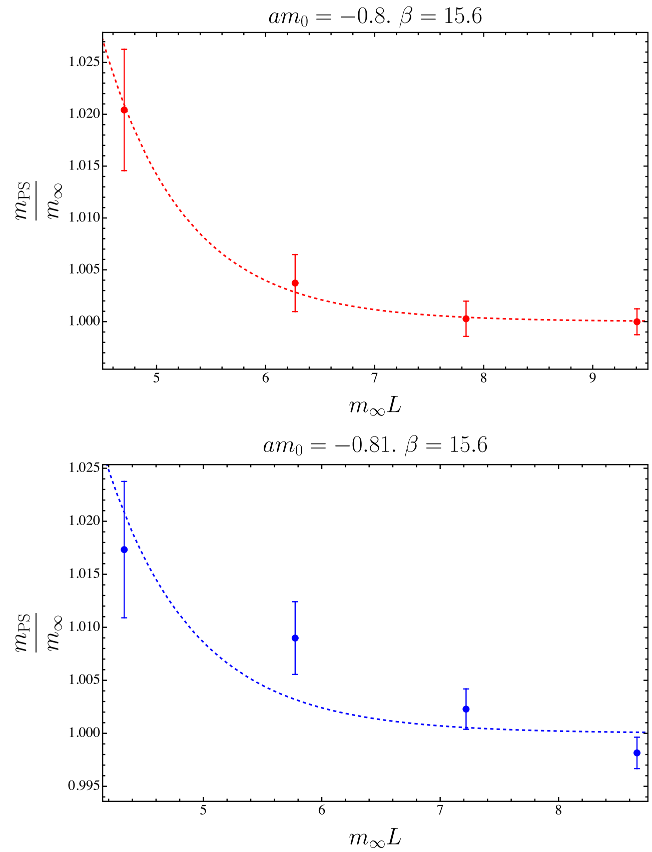

FIG. 4. Masses of PS mesons made of (f) fermions in the $Sp(6)$ theory, plotted as a function of $m_{\rm PS}L$, where $L = N_s a$ is the extent of the spatial lattice direction, for two representative choices of fermion mass. We normalize the mass to its infinite volume extrapolation ($m_{\rm PS}/m_\infty$). The dashed line is the prediction based on the infinite volume formula; $1 + A\frac{e^{-m_\infty L}}{(m_\infty L)^{3/2}}$, where A and m_∞ are fitting parameters.

restricting the sums to the lightest state in each channel. Our numerical results do not support saturation, as we shall see.

An extension of the sum rules is given by the quantity,

$$S \equiv 4\pi \sum_i \left(\frac{\hat{f}^2_{{\rm V},i}}{\hat{m}^2_{{\rm V},i}} - \frac{\hat{f}^2_{{\rm AV},i}}{\hat{m}^2_{{\rm AV},i}} \right), \tag{25}$$

where, again, the sum runs over all the states in the V and AV channels. In the case of a 2-flavor QCD-like theory, this is one of the many, equivalent, definitions of the Peskin-Takeuchi precision parameter, S [190], if we interpret the underlying dynamics in terms of a technicolor model of electroweak symmetry breaking. Interestingly, this quantity is dimensionless, therefore does not depend on the scale-setting procedure adopted. Extrapolating to small Higgs masses the combination of indirect tests of the electroweak theory, following Ref. [191], yields a conservative bound $|S| \lesssim 0.4$, at the 3σ confidence level. We can only provide a rough estimate for this quantity, obtained by saturating the defining sum with the first resonance, as is the case for the Weinberg sum rules, reminding the reader that, since this has not proved to be a valid approximation in the latter case, the result should be taken with a grain of salt.

For ease of comparison, we define three dimensionless quantities, involving only the lightest states:

$$s_0 \equiv 4\pi \left(\frac{\hat{f}^2_{\rm V}}{\hat{m}^2_{\rm V}} - \frac{\hat{f}^2_{\rm AV}}{\hat{m}^2_{\rm AV}} \right), \tag{26}$$

$$s_1 \equiv 1 - \frac{\hat{f}^2_{\rm AV} + \hat{f}^2_{\rm PS}}{\hat{f}^2_{\rm V}}, \tag{27}$$

$$s_2 \equiv 1 - \frac{\hat{m}^2_{\rm AV}\hat{f}^2_{\rm AV}}{\hat{m}^2_{\rm V}\hat{f}^2_{\rm V}}. \tag{28}$$

We compute them with massless and continuum limit extrapolations, and report the results in Table VII. The numerical evidence we collected indicates that neither s_1 nor s_2 vanish, which would discourage one from

TABLE VI. Massless and continuum extrapolation of the decay constants, $\hat{f}$, and masses, $\hat{m}$, expressed in units of the gradient flow scale, w_0, for quenched mesons, extrapolated to the $Sp(\infty)$ theory, for the three representations considered in this study. The uncertainties reported are determined by the extrapolation, starting from the statistical uncertainties of the individual measurements. Reduced chi-squared values, $\chi^2/N_{\mathrm{d.o.f.}}$, that are greater than 3.0 are highlighted in bold (e.g., 3.29). When the large-N extrapolation has been performed with only two data points, this has been done by simple error propagation, solving for the coefficients of a linear extrapolation. Only statistical uncertainties have been included. A few extrapolations for the heaviest states made of fermions in large representations result in negative values of mass squared, due to the existence of large systematic errors affecting these few observables. The large-N extrapolation for (as) and (s) fermions do not agree, except for the pseudoscalar decay constant, as discussed in the main body of the paper.

	$Sp(\infty)$		
Representation	Channel	Chiral limit	χ^2/d.o.f.
Fundamental	$\hat{f}^2_{\mathrm{PS}}/N_c$	0.01913(77)	**3.29**
	$\hat{f}^2_{\mathrm{V}}/N_c$	0.0523(50)	1.31
	$\hat{f}^2_{\mathrm{AV}}/N_c$	0.073(16)	0.00
	$\hat{m}^2_{\mathrm{V}}$	0.307(15)	0.08
	$\hat{m}^2_{\mathrm{AV}}$	0.84(22)	0.29
	$\hat{m}^2_{\mathrm{S}}$	0.28(18)	1.25
	$\hat{m}^2_{\mathrm{T}}$	0.315(25)	**3.36**
	$\hat{m}^2_{\mathrm{AT}}$	0.62(26)	0.58
Antisymmetric	$\hat{f}^2_{\mathrm{ps}}/N_c^2$	0.0851(26)	2.68
	$\hat{f}^2_{\mathrm{v}}/N_c^2$	0.323(26)	0.60
	$\hat{f}^2_{\mathrm{av}}/N_c^2$	0.085(43)	...
	$\hat{m}^2_{\mathrm{v}}$	0.710(24)	0.04
	$\hat{m}^2_{\mathrm{av}}$	−0.07(60)	...
	$\hat{m}^2_{\mathrm{s}}$	−0.14(47)	...
	$\hat{m}^2_{\mathrm{t}}$	0.705(36)	0.83
	$\hat{m}^2_{\mathrm{at}}$	2.50(93)	...
Symmetric	$\hat{f}^2_{\mathcal{PS}}/N_c^2$	0.0901(45)	0.01
	$\hat{f}^2_{\mathcal{V}}/N_c^2$	0.730(35)	**20.18**
	$\hat{f}^2_{\mathcal{AV}}/N_c^2$	0.22(11)	...
	$\hat{m}^2_{\mathcal{V}}$	1.033(28)	1.93
	$\hat{m}^2_{\mathcal{AV}}$	−1.10(71)	...
	$\hat{m}^2_{\mathcal{S}}$	−1.94(37)	...
	$\hat{m}^2_{\mathcal{T}}$	1.033(40)	**5.77**
	$\hat{m}^2_{\mathcal{AT}}$	−0.8(.6)	...

using the approximation of saturating the sum rules on the first resonance only. These results suggest to use caution, as in general s_0 will also differ from S. It would be interesting to repeat this exercise with lattice calculations that involve dynamical fermions, to see how the dynamics affects them. For completeness, and to facilitate comparison, we include in the table also the estimates of the same quantities for 2-flavor QCD, for which we borrow the input from Table II of Ref. [188], based in turn on data from Ref. [192], even if these numerical results are obtained with a nonzero mass for the quarks ($m_\pi = 139.6$ MeV): $f_\pi = 92.4 \pm 0.35$ MeV, $f_\rho = 153.4 \pm 7.2$ MeV, $f_{a_1} = 152.4 \pm 10.4$ MeV, $m_\rho = 775.8 \pm 0.5$ MeV, $m_{a_1} = 1230 \pm 40$ MeV.

TABLE VII. Numerical results for the sum rules s_0, s_1, and s_2, as defined in the main text, which include only the lightest bound states. All results for $Sp(2N)$ use extrapolations to the massless and continuum limits of the (quenched) theories discussed in the body of the paper. The $SU(3)$ case is included for comparison, and uses numerical values from Ref. [188] and references therein, for finite mass of the two (f) fermions. The uncertainties are computed with simple error propagation, ignoring correlations. The $Sp(8)$ case is incomplete, as some measurements are missing, as explained in the main text.

Theory	s_0	s_1	s_2
$Sp(4)$, (f)	0.397(75)	−1.07(21)	−4.88(82)
$Sp(4)$, (as)	0.33(10)	−1.08(28)	−4.09(94)
$Sp(4)$, (s)	0.26(18)	−1.48(31)	−4.95(99)
$Sp(6)$, (f)	0.72(15)	−0.81(25)	−3.88(94)
$Sp(6)$, (as)	1.70(35)	0.12(14)	0.01(26)
$Sp(6)$, (s)	1.25(63)	−0.00(17)	−0.02(28)
$Sp(8)$, (f)	0.62(19)	−0.96(30)	−3.8(1.0)
$Sp(8)$, (as)	...	...	...
$Sp(8)$, (s)	...	...	...
$Sp(\infty)$, (f)	1.04(44) N_c	−0.77(35)	−2.8(1.4)
$Sp(\infty)$, (as)	$0.2(1.5) \times 10^2\ N_c^2$	0.47(14)	1.02(22)
$Sp(\infty)$, (s)	11.3(2.1) N_c^2	0.58(15)	1.31(26)
$SU(3)$, (f) ($m_\pi = 139.6$ MeV)	0.298(55)	−0.35(18)	−1.48(44)

IV. CONCLUSIONS AND OUTLOOK

We reported the results of a first systematic study of the spectra of mesons in $Sp(2N)$ lattice gauge theories with fermions in three different representations, in the quenched approximation, for $N = 2$, 3, 4. We applied next-to-leading-order WχPT to extract the continuum and massless limits of the spectroscopy observables. We also performed a first simplified extrapolation towards the large-N limit. Finally, we computed nontrivial quantities, related to the Weinberg sum rules, using the lattice numerical results, with the additional drastic approximation of including only the ground states. For all these measurements, we also performed an extensive exploration of the lattice parameter space, to assess the magnitude of finite-size effects. Details about the intermediate steps of these calculations can be found in the public releases in Ref. [185].

In principle, our results are applicable to phenomenological studies of models of new physics that extend the standard model, particularly when the number of fermion species is small, and when the quenched approximation is sufficient to provide useful estimates of masses and decay constants for the mesons. This includes the context of composite Higgs models and models of dark matter with strong-coupling origin. However, the systematics highlighted in our discussion, which affect more severely some of the states we have analyzed, would suggest to exercise judicious caution if using these results for phenomenological applications.

This study sets the stage for future, extensive and high precision measurements of spectroscopy observables in the corresponding lattice gauge theories with dynamical fermions, by benchmarking the lattice parameter space. A first study of the spectrum of fermion bound states (chimera baryons), that have model-building relevance in the context of top partial compositeness, performed in the quenched approximation and for $Sp(4)$ gauge theories, can be found in Ref. [193]. An ongoing, extensive research program of study of the dynamical theories with fermions transforming in multiple representations will provide precision measurements and explore complementary regions of parameter space, relevant for some phenomenological applications, for which one does not expect the quenched approximation to hold.

Full raw data for correlation functions and gradient-flow histories, and all data presented in plots and tables in this work, can be downloaded in machine-readable format at Ref. [185]. The analysis workflow used to generate the latter from the former, and to produce the plots and tables presented in this work, can be downloaded at Ref. [194].

ACKNOWLEDGMENTS

The work of E. B. has been funded by the Supercomputing Wales project, which is part-funded by the European Regional Development Fund (ERDF) via Welsh Government and by the UKRI Science and Technologies Facilities Council (STFC) Research Software Engineering Fellowship EP/V052489/1. J. H. is partially supported by the Center for Frontier Nuclear Science at Stony Brook University. The work of D. K. H. was supported by Basic Science Research Program through the National Research Foundation of Korea (NRF) funded by the Ministry of Education (NRF-2017R1D1A1B06033701) and also by the Korea government (MSIT) (2021R1A4A5031460). The work of J.-W. L. was supported in part by the National Research Foundation of Korea (NRF) grant funded by the Korea government (MSIT) (NRF-2018R1C1B3001379) and by IBS under the Project Code No. IBS-R018-D1. The work of C.-J. D. L. and of H. H. is supported by the Taiwanese NTSC Grant No. 112-2112-M-A49-021-MY3. The work of B. L. and M. P. has been supported in part by the STFC Consolidated Grants No. ST/P00055X/1, No. ST/T000813/1, and No. ST/X000648/1. B. L. and M. P. received funding from the European Research Council (ERC) under the European Union's Horizon 2020 research and innovation program under Grant Agreement No. 813942. The work of B. L. is further supported in part by the Royal Society Wolfson Research Merit Award No. WM170010 and by the Leverhulme Trust Research Fellowship No. RF-2020-4619. The work of D. V. is supported by STFC under the consolidated Grant No. ST/X000680/1. Numerical simulations have been performed on the Swansea SUNBIRD cluster (part of the Supercomputing Wales project) and AccelerateAI A100 GPU system. The Swansea SUNBIRD system and AccelerateAI are part funded by the European Regional Development Fund (ERDF) via Welsh Government.

APPENDIX A: FINITE VOLUME EFFECTS

Finite size effects arise from the limited extent of the lattice as well as its toroidal nature. These artifacts can contaminate our measurements of observable quantities. It is possible to extrapolate to infinite volume (the analog of the thermodynamic limit of statistical mechanics) from a lattice of finite extent, $L = N_s a$, by assuming that the mass of the lightest state at finite volume, which we denote generically as m_π in this Appendix, is related to the infinite-volume limit, m_∞, via the relation,

$$m_\pi = m_\infty \left(1 + A \frac{e^{-m_\infty L}}{(m_\infty L)^{3/2}}\right) \tag{A1}$$

first established in Ref. [195].

As a preliminary study, propaedeutic to the one reported in the body of this paper, we examined the finite-size effect by plotting m_π/m_∞ as a function of $m_\infty L$ as emerges from different lattice volumes as well as with different bare masses, m_0, for the relevant fermion. We choose the value of $m_\infty L$ such that the finite volume result is within a few per mille of the infinite volume one, such that this source of systematics can be ignored in comparison with the statistical uncertainties. Details about this study can be found in Refs. [185,194], while here we only provide one example, in Fig. 4, for the $Sp(6)$ theory.

The finite size effects for $Sp(4)$ quenched mesons in the fundamental and antisymmetric representations were studied in Ref. [122], and it was found that one should restrict the analysis to cases in which $m_\pi L \gtrsim 7.5$ for both fundamental and antisymmetric representations, with the identification $m_\pi = m_{\mathrm{PS}}$. Interestingly, we find that this requirement is even more severe for the $Sp(6)$ and $Sp(8)$ theories. The ensembles and choice of fermions masses used in the analysis the forms the body of this paper are lead to satisfying these requirements. To prevent nonphysical processes, such as the analogous process to

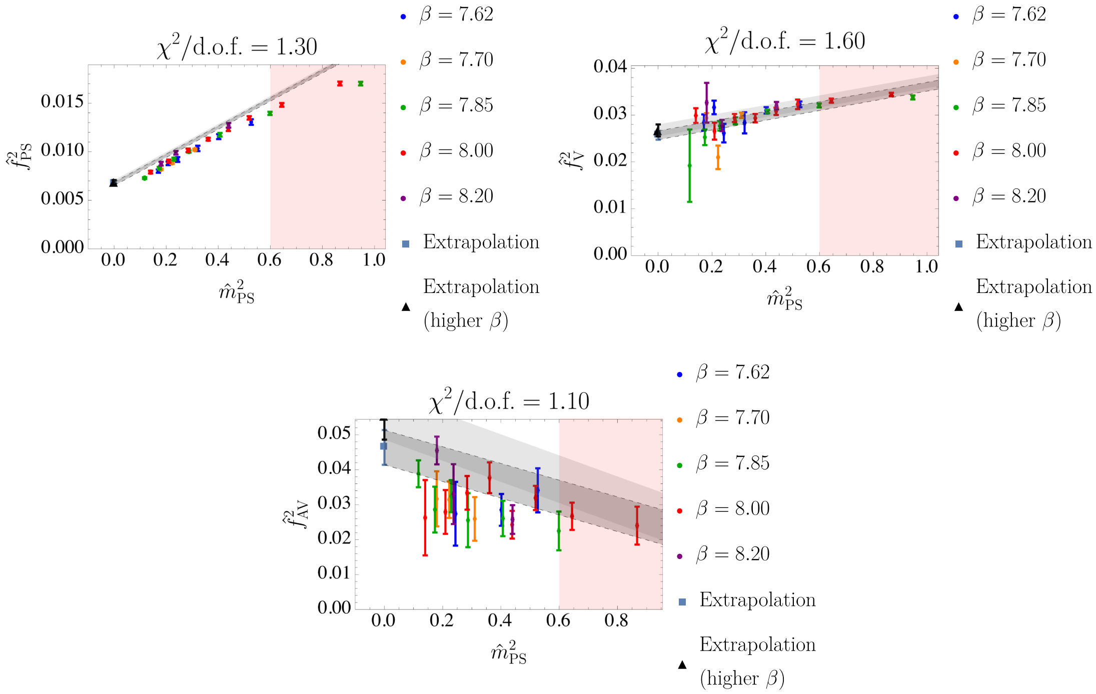

FIG. 5. Decay constants squared in the PS, V, and AV channels comprised of fermions in the fundamental representation of $Sp(4)$. The reduced chi-squared value is printed at the top of each plot. Data points in the pink shaded region are not included in the curve-fitting procedure. The gray band represents the continuum and massless extrapolation, with the blue square being the observable and the vertical width corresponding to the statistical error. In instances where a reliable extrapolation cannot be made, no gray band is shown. All quantities are expressed in units of the gradient flow scale, w_0. The extrapolation with the smallest β value removed is shown as a lighter gray band and a black triangle in cases where data were available at the smallest β value.

the $\rho \to \pi\pi$ decay, we also demand that $0.5 < m_{\rm PS}/m_{\rm V} < 1$, for all fermion species, so that the quenched approximation can be justified.

APPENDIX B: CONTINUUM AND MASSLESS EXTRAPOLATIONS

Having computed (quenched) meson masses and decay constants in a discrete spacetime lattice at finite bare mass, we then extrapolate to the continuum and massless limits simultaneously, by means of next-to-leading-order WχPT. We plot our measurements, and the extrapolations, for $Sp(4)$, $Sp(6)$ and $Sp(8)$ in Figs. 5–22, while the numerical details can be found in Refs. [185,194]. For the extrapolations to the massless limit, we have excluded the points for which $\hat{f}_{\rm PS}$ does not exhibit a linear behavior in $\hat{m}_{\rm PS}$. We exclude this set of points from all massless extrapolations at fixed N and representation.

In a similar spirit, we display our large-N extrapolations of the massless and continuum extrapolations, for all three fermion representations, in Figs. 23–28, while intermediate results and the complete set of fitted parameters can be downloaded from Ref. [185].

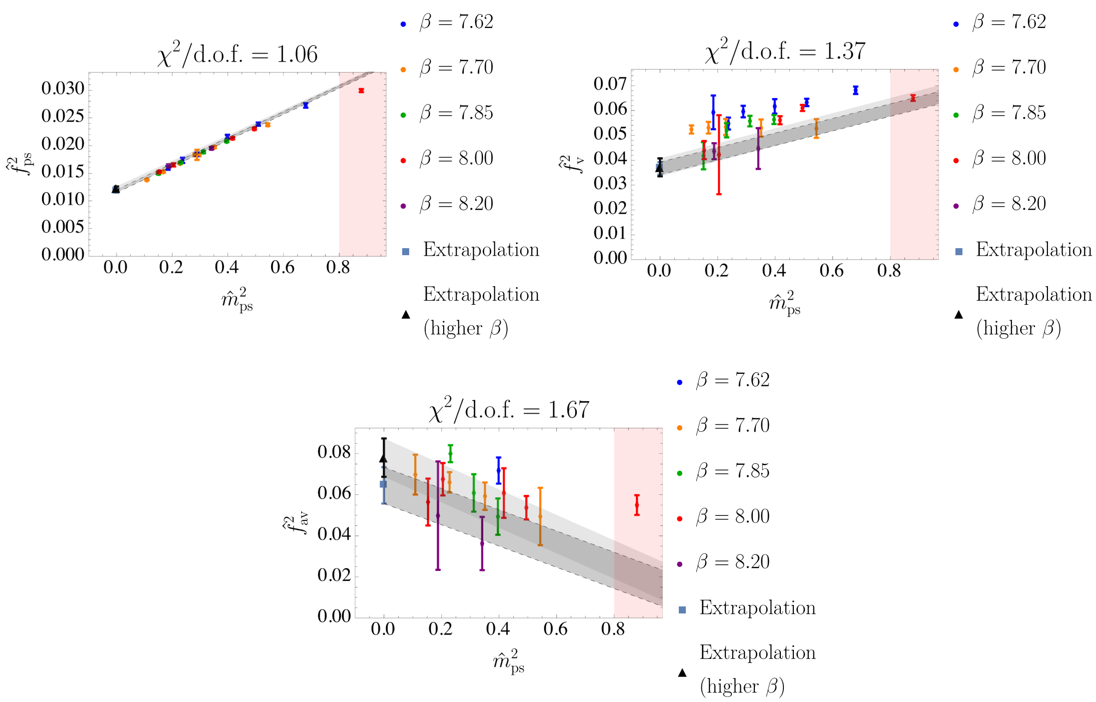

FIG. 6. Decay constants squared in the ps, v, and av channels comprised of fermions in the antisymmetric representation of $Sp(4)$. The reduced chi-squared value is printed at the top of each plot. Data points in the pink shaded region are not included in the curve-fitting procedure. The gray band represents the continuum and massless extrapolation with the blue square being the observable and the vertical width corresponding to the statistical error. In instances where a reliable extrapolation cannot be made, no gray band is shown. All quantities are expressed in units of the gradient flow scale, w_0. The extrapolation with the smallest β value removed is shown as a lighter gray band and a black triangle in cases where data were available at the smallest β value.

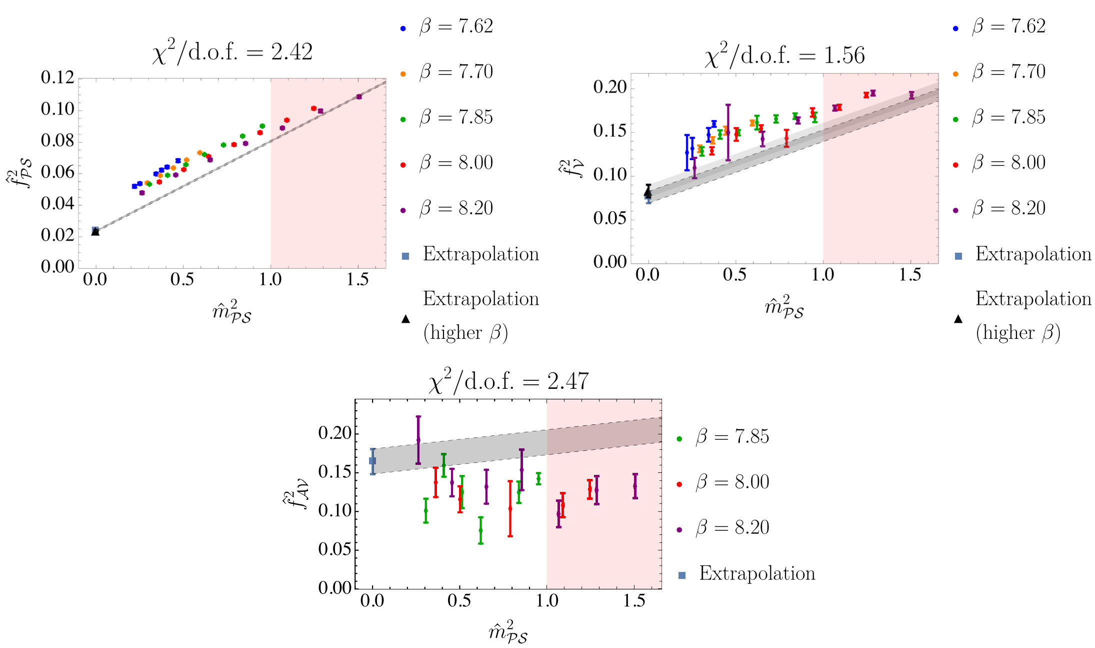

FIG. 7. Decay constants squared in the $\mathcal{PS}$, $\mathcal{V}$, and $\mathcal{AV}$ channels comprised of fermions in the symmetric representation of $Sp(4)$. The reduced chi-squared value is printed at the top of each plot. Data points in the pink shaded region are not included in the curve-fitting procedure. The gray band represents the continuum and massless extrapolation with the blue square being the observable and the vertical width corresponding to the statistical error. In instances where a reliable extrapolation cannot be made, no gray band is shown. All quantities are expressed in units of the gradient flow scale, w_0. The extrapolation with the smallest β value removed is shown as a lighter gray band and a black triangle in cases where data were available at the smallest β value.

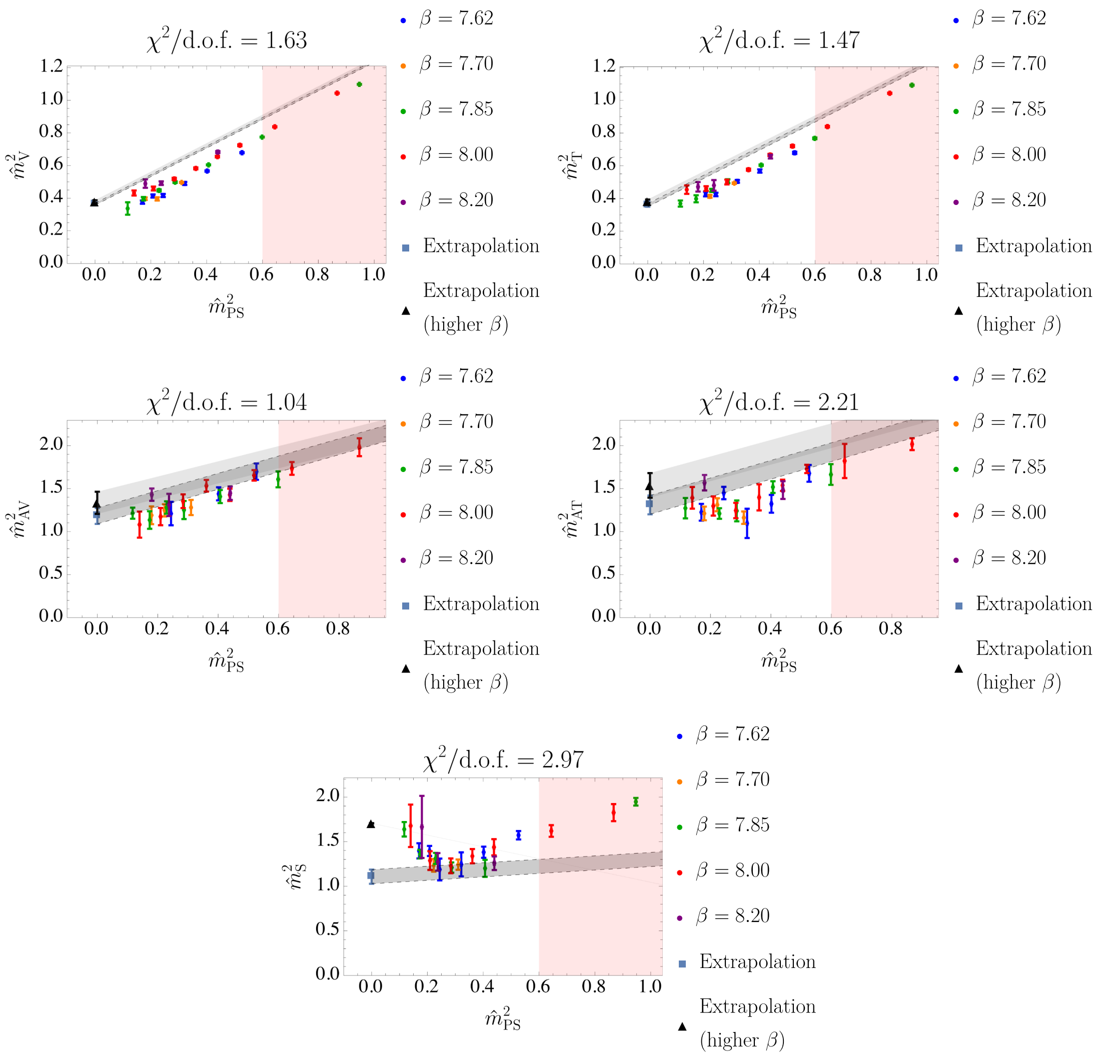

FIG. 8. Masses squared in the V, T, AV, AT, and S channels comprised of fermions in the fundamental representation of $Sp(4)$. The reduced chi-squared value is printed at the top of each plot. Data points in the pink shaded region are not included in the curve-fitting procedure. The gray band represents the continuum and massless extrapolation with the blue square being the observable and the vertical width corresponding to the statistical error. In instances where a reliable extrapolation cannot be made, no gray band is shown. All quantities are expressed in units of the gradient flow scale, w_0. The extrapolation with the smallest β value removed is shown as a lighter gray band and a black triangle in cases where data were available at the smallest β value.

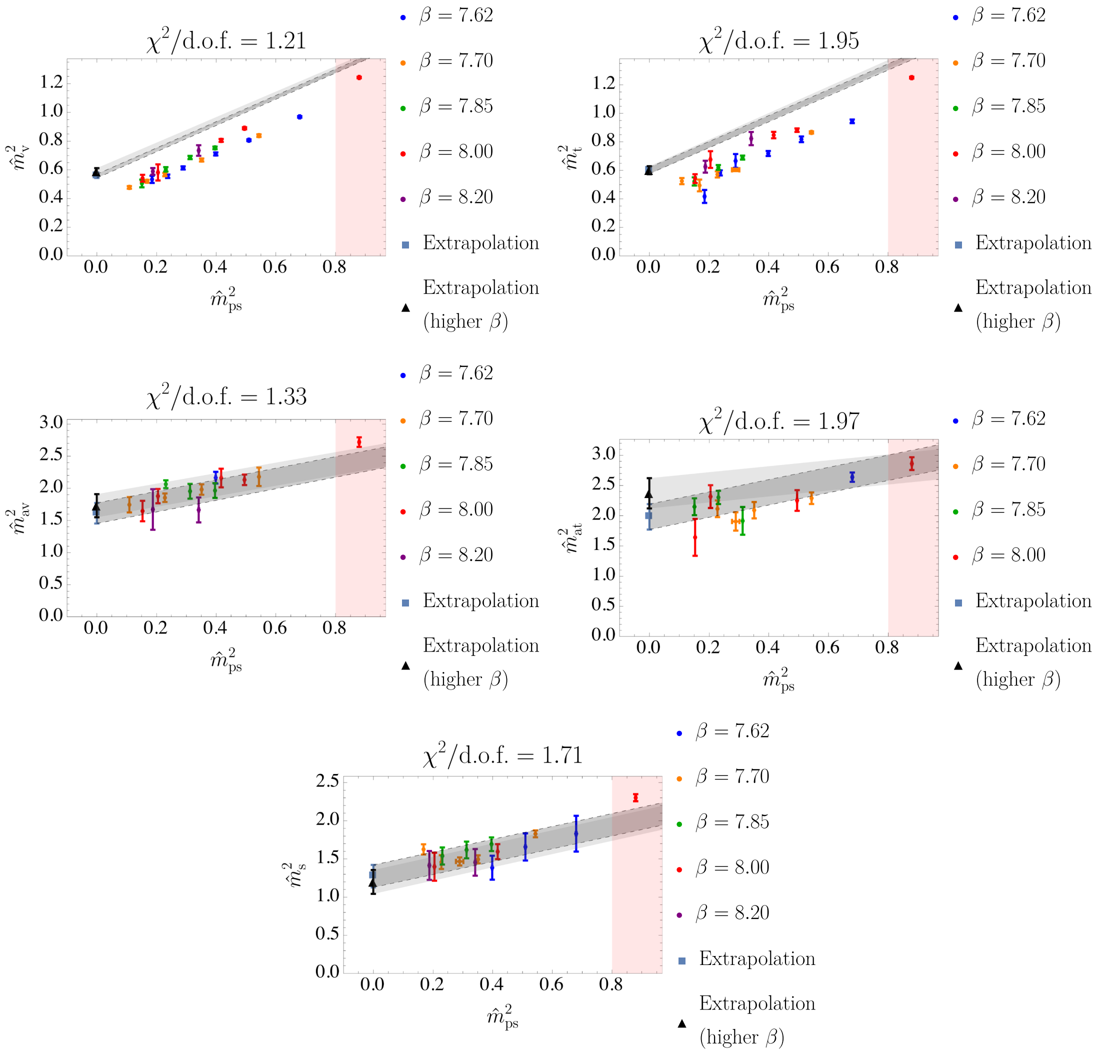

FIG. 9. Masses squared in the v, t, av, at, and s channels comprised of fermions in the antisymmetric representation of $Sp(4)$. The reduced chi-squared value is printed at the top of each plot. Data points in the pink shaded region are not included in the curve-fitting procedure. The gray band represents the continuum and massless extrapolation with the blue square being the observable and the vertical width corresponding to the statistical error. In instances where a reliable extrapolation cannot be made, no gray band is shown. All quantities are expressed in units of the gradient flow scale, w_0. The extrapolation with the smallest β value removed is shown as a lighter gray band and a black triangle in cases where data were available at the smallest β value.

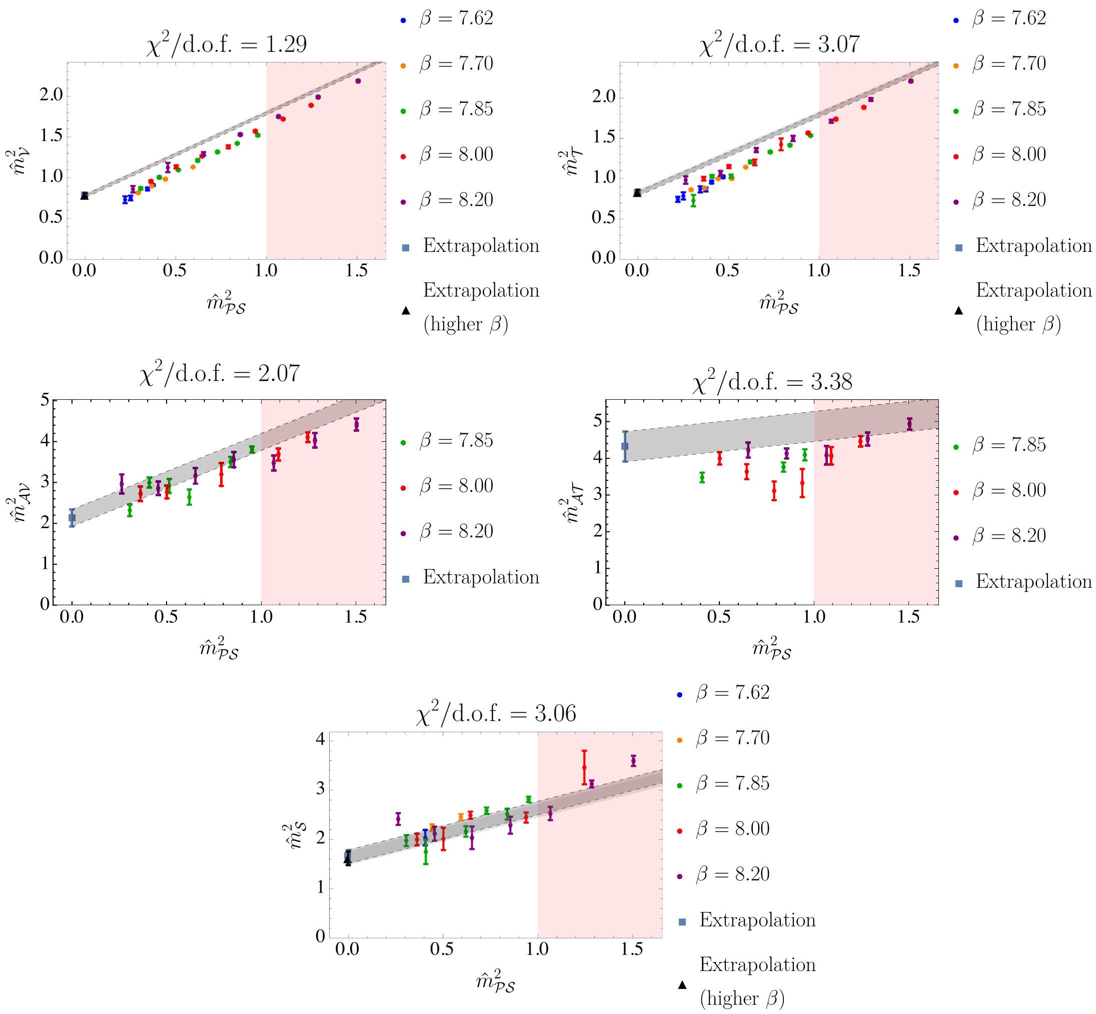

FIG. 10. Masses squared in the $\mathcal{V}$, $\mathcal{T}$, $\mathcal{AV}$, $\mathcal{AT}$ and $\mathcal{S}$ channels comprised of fermions in the symmetric representation of $Sp(4)$. The reduced chi-squared value is printed at the top of each plot. Data points in the pink shaded region are not included in the curve-fitting procedure. The gray band represents the continuum and massless extrapolation with the blue square being the observable and the vertical width corresponding to the statistical error. In instances where a reliable extrapolation cannot be made, no gray band is shown. All quantities are expressed in units of the gradient flow scale, w_0. The extrapolation with the smallest β value removed is shown as a lighter gray band and a black triangle in cases where data were available at the smallest β value.

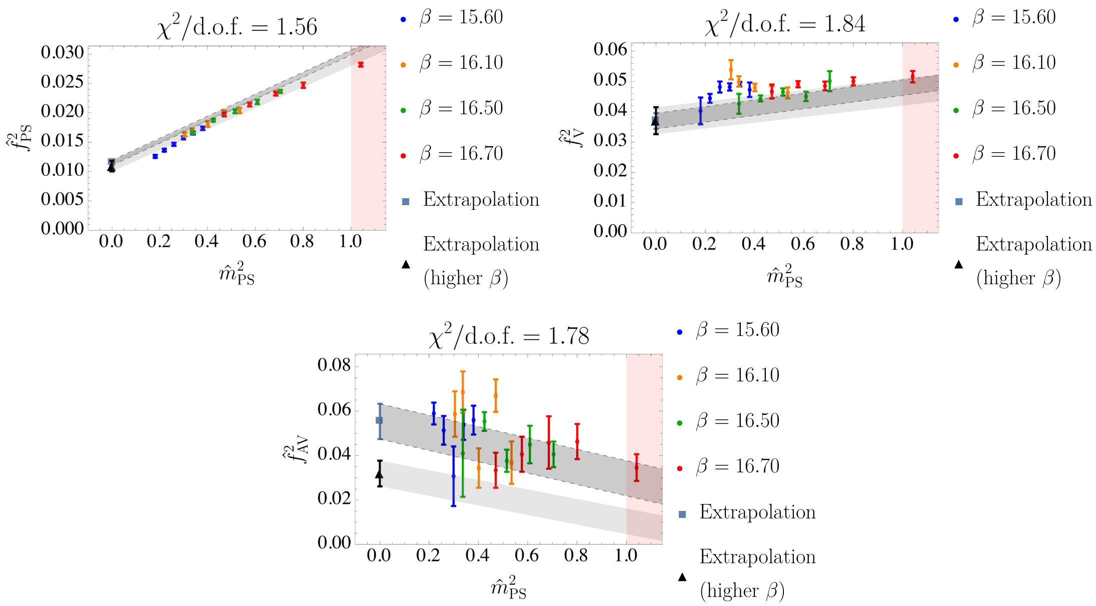

FIG. 11. Decay constants squared in the PS, V, and AV channels comprised of fermions in the fundamental representation of $Sp(6)$. The reduced chi-squared value is printed at the top of each plot. Data points in the pink shaded region are not included in the curve-fitting procedure. The gray band represents the continuum and massless extrapolation with the blue square being the observable and the vertical width corresponding to the statistical error. In instances where a reliable extrapolation cannot be made, no gray band is shown. All quantities are expressed in units of the gradient flow scale, w_0. The extrapolation with the smallest β value removed is shown as a lighter gray band and a black triangle in cases where data were available at the smallest β value.

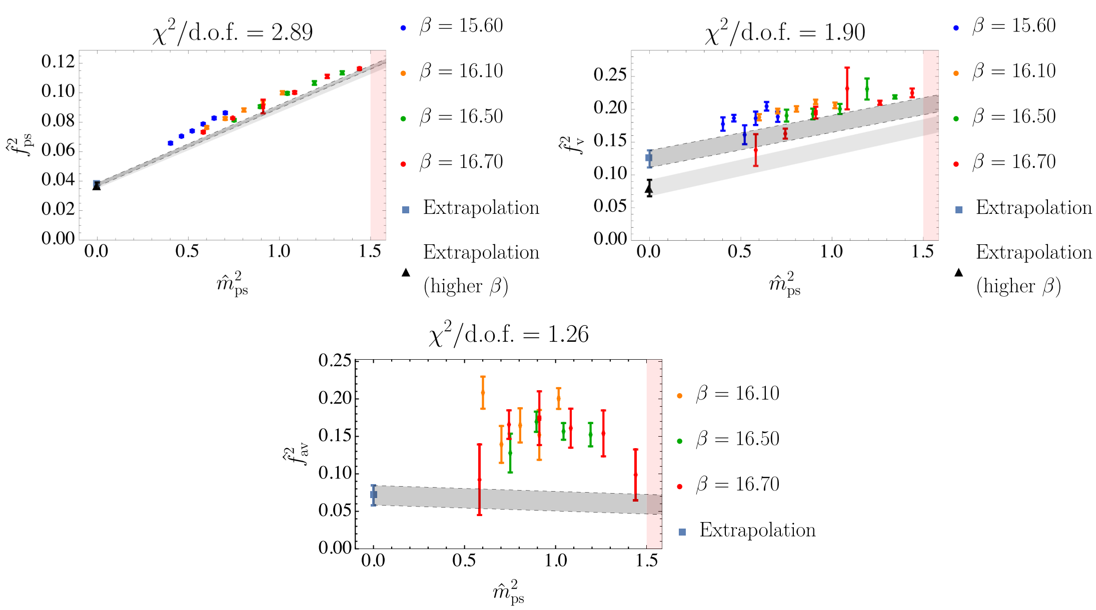

FIG. 12. Decay constants squared for ps, v, and av channels comprised of fermions in the antisymmetric representation of $Sp(6)$. The reduced chi-squared value is printed at the top of each plot. Data points in the pink shaded region are not included in the curve-fitting procedure. The gray band represents the continuum and massless extrapolation with the blue square being the observable in the massless limit and the vertical width corresponding to the statistical error. In instances where a reliable extrapolation cannot be made, no gray band is shown. All quantities are expressed in units of the gradient flow scale, w_0. The extrapolation with the smallest β value removed is shown as a lighter gray band and a black triangle in cases where data were available at the smallest β value.

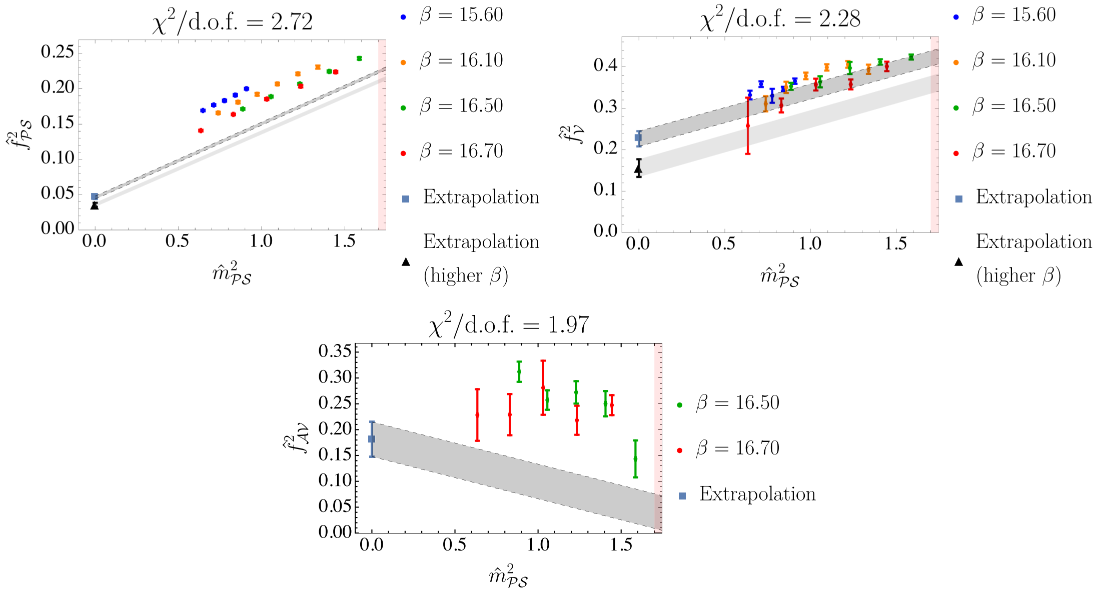

FIG. 13. Decay constants squared in the $\mathcal{PS}$, $\mathcal{V}$, and $\mathcal{AV}$ channels comprised of fermions in the symmetric representation of $Sp(6)$. The reduced chi-squared value is printed at the top of each plot. Data points in the pink shaded region are not included in the curve-fitting procedure. The gray band represents the continuum and massless extrapolation with the blue square being the observable and the vertical width corresponding to the statistical error. In instances where a reliable extrapolation cannot be made, no gray band is shown. All quantities are expressed in units of the gradient flow scale, w_0. The extrapolation with the smallest β value removed is shown as a lighter gray band and a black triangle in cases where data were available at the smallest β value.

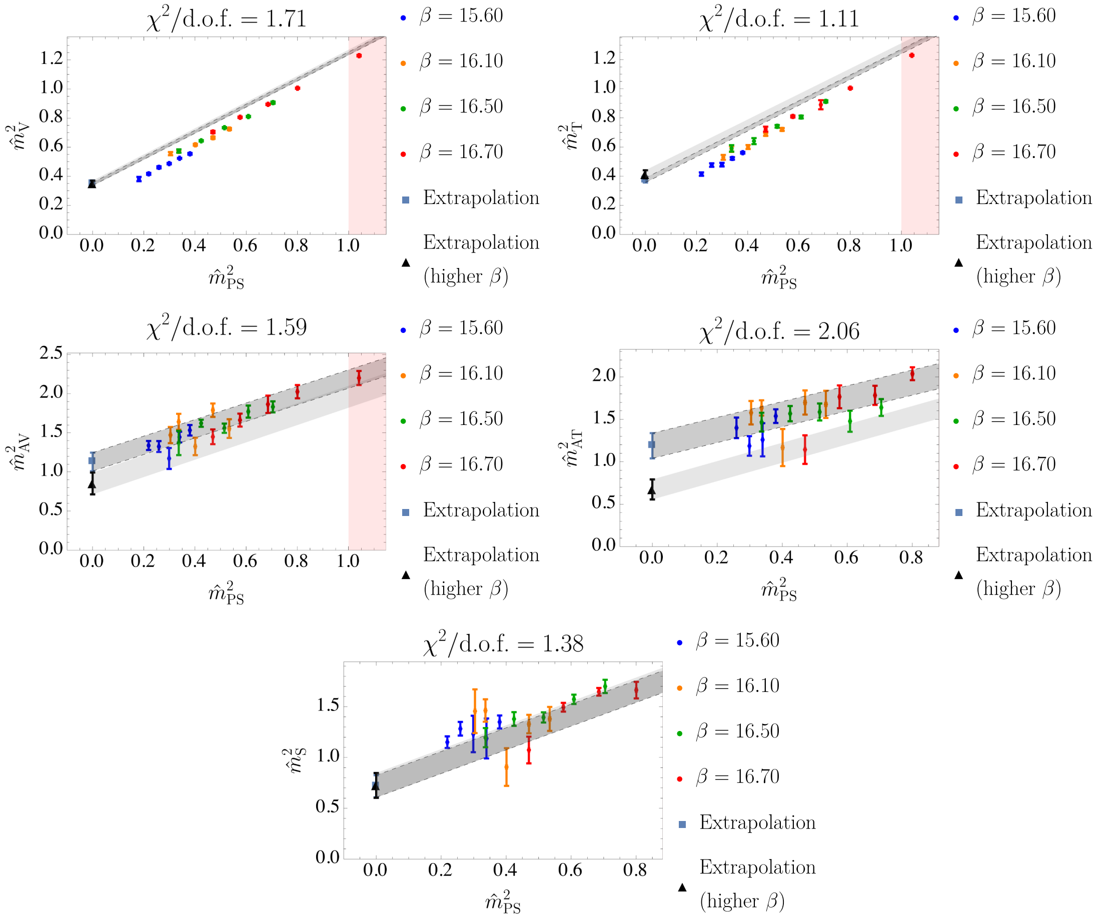

FIG. 14. Masses squared in the V, T, AV, AT, and S channels comprised of fermions in the fundamental representation of $Sp(6)$. The reduced chi-squared value is printed at the top of each plot. Data points in the pink shaded region are not included in the curve-fitting procedure. The gray band represents the continuum and massless extrapolation with the blue square being the observable and the vertical width corresponding to the statistical error. In instances where a reliable extrapolation cannot be made, no gray band is shown. All quantities are expressed in units of the gradient flow scale, w_0. The extrapolation with the smallest β value removed is shown as a lighter gray band and a black triangle in cases where data were available at the smallest β value.

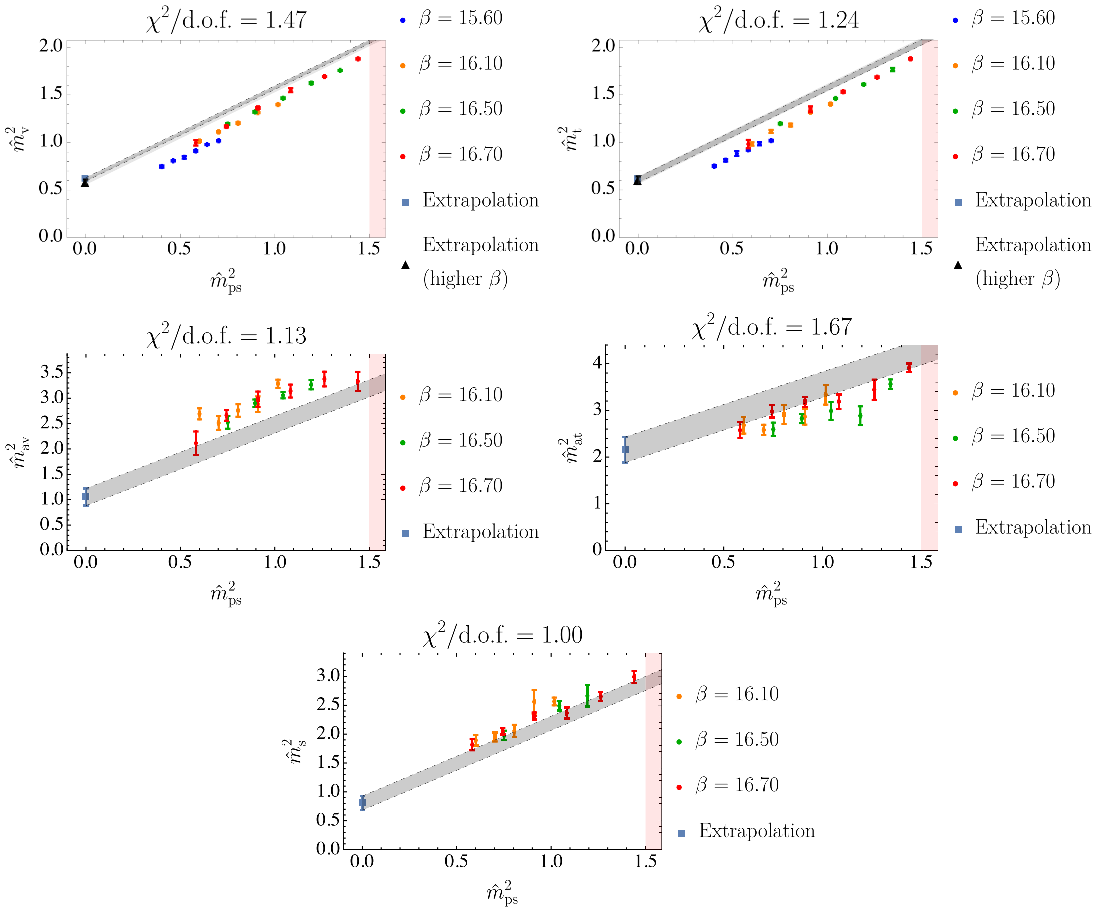

FIG. 15. Masses squared in the v, t, av, at, and s channels comprised of fermions in the antisymmetric representation of $Sp(6)$. The reduced chi-squared value is printed at the top of each plot. Data points in the pink shaded region are not included in the curve-fitting procedure. The gray band represents the continuum and massless extrapolation with the blue square being the observable and the vertical width corresponding to the statistical error. In instances where a reliable extrapolation cannot be made, no gray band is shown. All quantities are expressed in units of the gradient flow scale, w_0. The extrapolation with the smallest β value removed is shown as a lighter gray band and a black triangle in cases where data were available at the smallest β value.

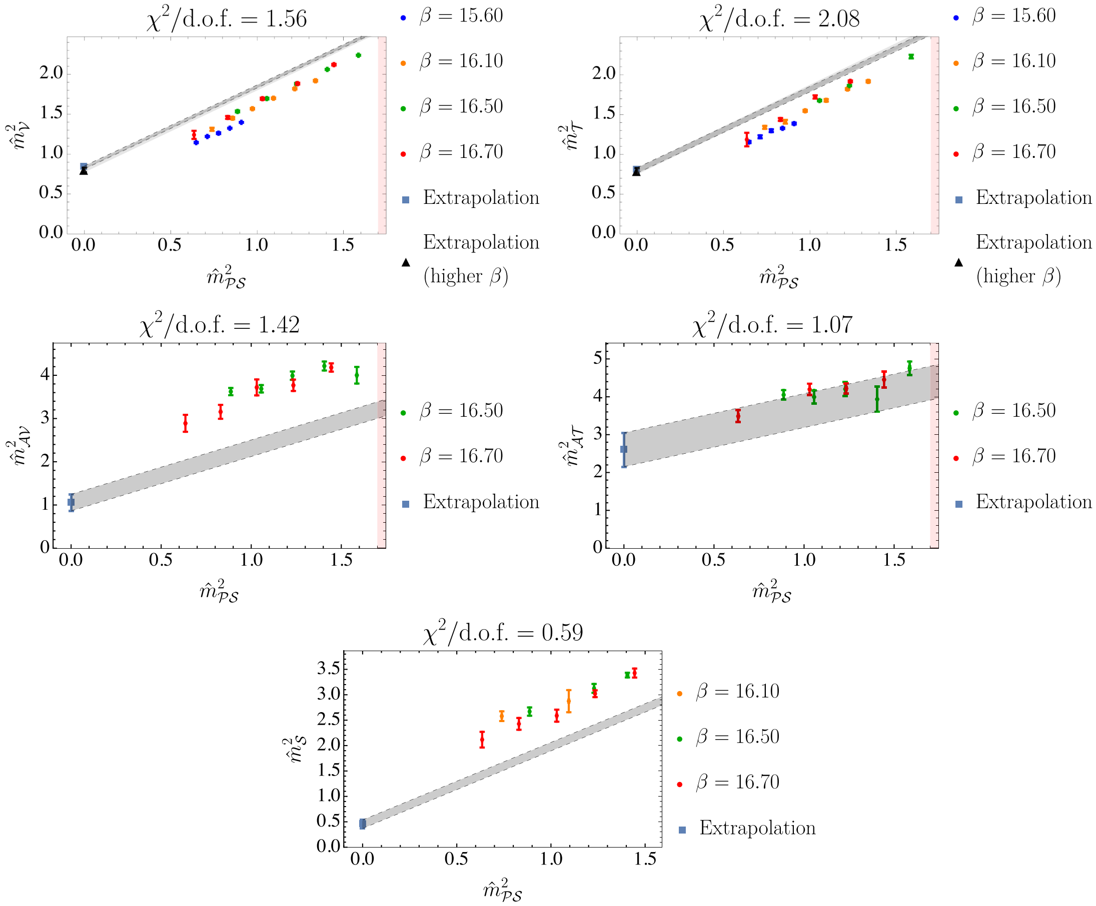

FIG. 16. Masses squared in the $\mathcal{V}$, $\mathcal{T}$, $\mathcal{AV}$, $\mathcal{AT}$ and $\mathcal{S}$ channels comprised of fermions in the symmetric representation of $Sp(6)$. The reduced chi-squared value is printed at the top of each plot. Data points in the pink shaded region are not included in the curve-fitting procedure. The gray band represents the continuum and massless extrapolation with the blue square being the observable and the vertical width corresponding to the statistical error. In instances where a reliable extrapolation cannot be made, no gray band is shown. All quantities are expressed in units of the gradient flow scale, w_0. The extrapolation with the smallest β value removed is shown as a lighter gray band and a black triangle in cases where data were available at the smallest β value.

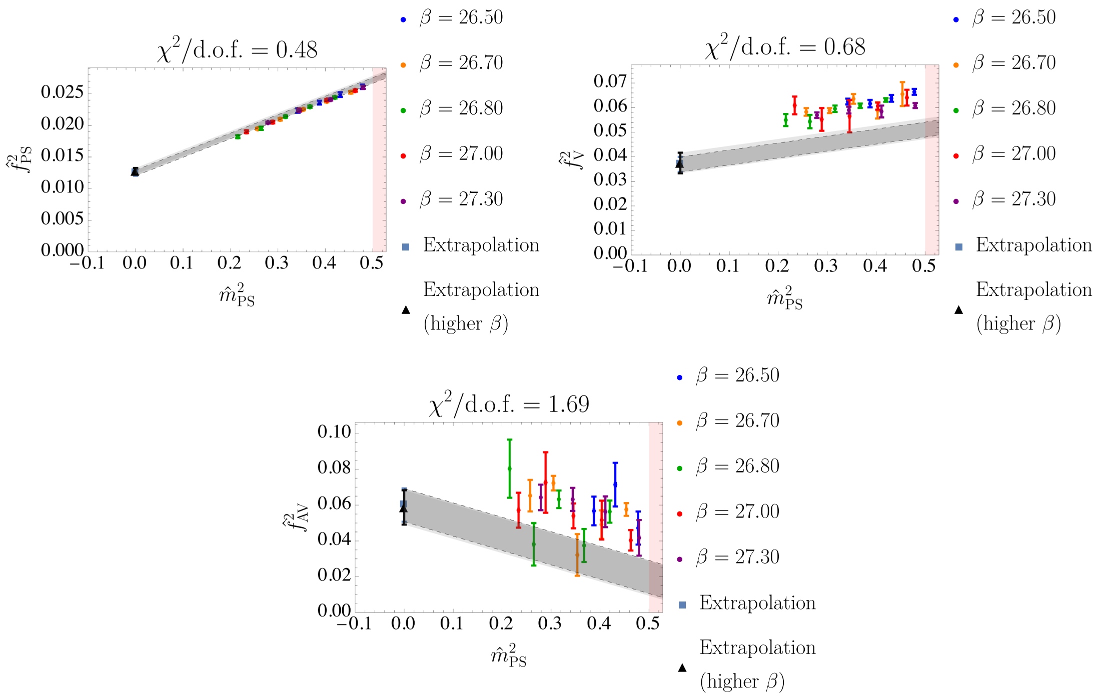

FIG. 17. Decay constants squared in the PS, V and AV channels comprised of fermions in the fundamental representation of $Sp(8)$. The reduced chi-squared value is printed at the top of each plot. Data points in the pink shaded region are not included in the curve-fitting procedure. The gray band represents the continuum and massless extrapolation with the blue square being the observable and the vertical width corresponding to the statistical error. In instances where a reliable extrapolation cannot be made, no gray band is shown. All quantities are expressed in units of the gradient flow scale, w_0. The extrapolation with the smallest β value removed is shown as a lighter gray band and a black triangle in cases where data were available at the smallest β value.

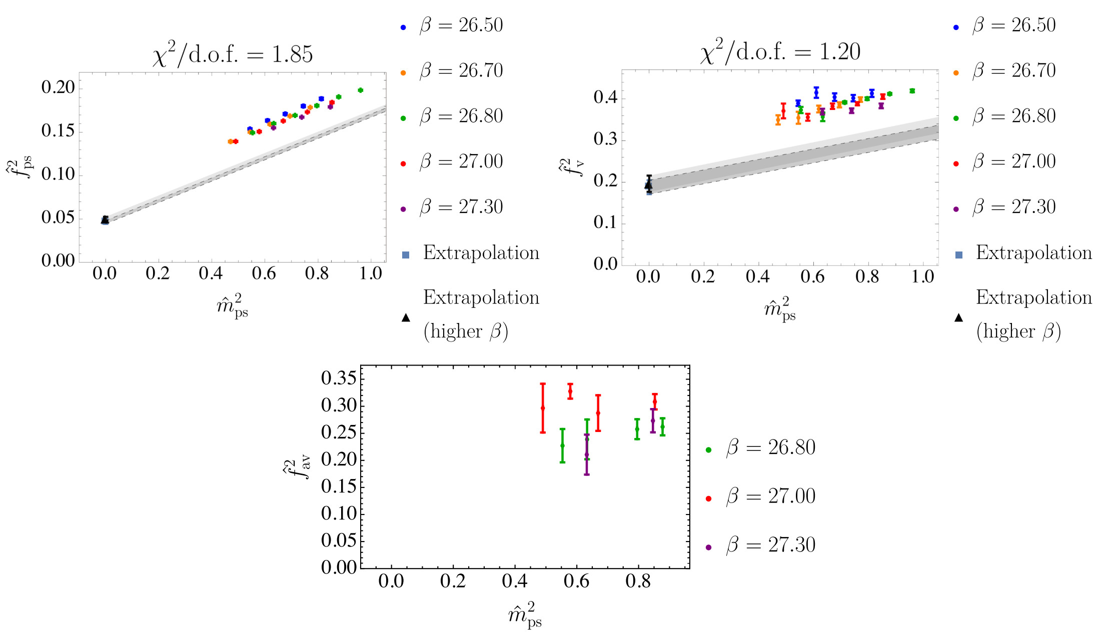

FIG. 18. Decay constants squared in the ps, v, and av channels comprised of fermions in the antisymmetric representation of $Sp(8)$. The reduced chi-squared value is printed at the top of each plot. Data points in the pink shaded region are not included in the curve-fitting procedure. The gray band represents the continuum and massless extrapolation with the blue square being the observable and the vertical width corresponding to the statistical error. In instances where a reliable extrapolation cannot be made, no gray band is shown. All quantities are expressed in units of the gradient flow scale, w_0. The extrapolation with the smallest β value removed is shown as a lighter gray band and a black triangle in cases where data were available at the smallest β value.

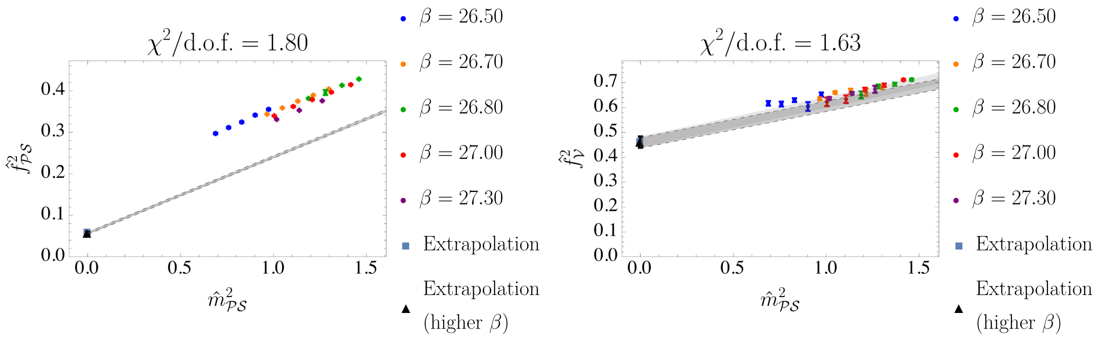

FIG. 19. Decay constants squared in the $\mathcal{PS}$ and $\mathcal{V}$ channels comprised of fermions in the symmetric representation of $Sp(8)$. The reduced chi-squared value is printed at the top of each plot. Data points in the pink shaded region are not included in the curve-fitting procedure. The gray band represents the continuum and massless extrapolation with the blue square being the observable and the vertical width corresponding to the statistical error. In instances where a reliable extrapolation cannot be made, no gray band is shown. All quantities are expressed in units of the gradient flow scale, w_0. The extrapolation with the smallest β value removed is shown as a lighter gray band and a black triangle in cases where data were available at the smallest β value.

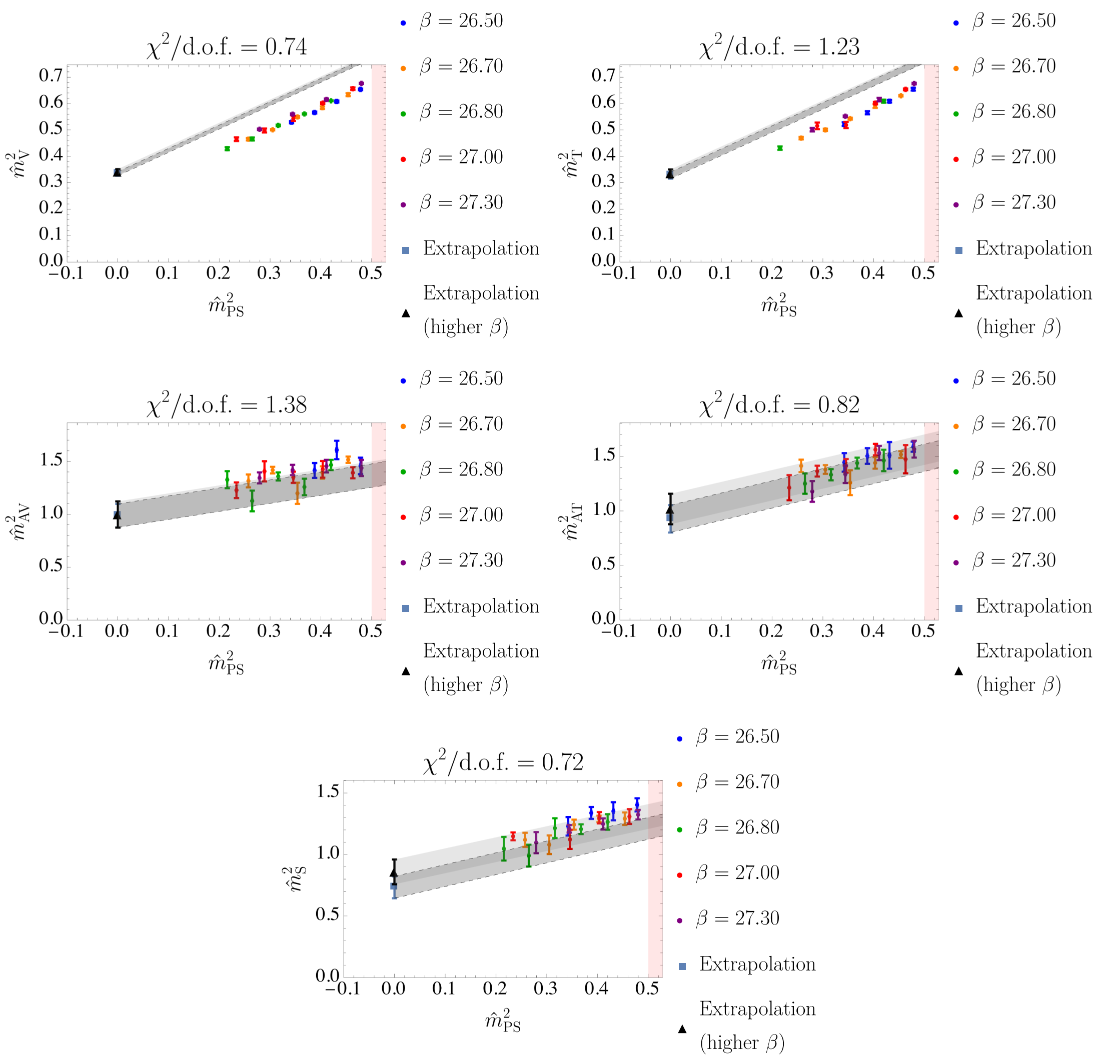

FIG. 20. Masses squared in the V, T, AV, AT, and S channels comprised of fermions in the fundamental representation of $Sp(8)$. The reduced chi-squared value is printed at the top of each plot. Data points in the pink shaded region are not included in the curve-fitting procedure. The gray band represents the continuum and massless extrapolation with the blue square being the observable and the vertical width corresponding to the statistical error. In instances where a reliable extrapolation cannot be made, no gray band is shown. All quantities are expressed in units of the gradient flow scale, w_0. The extrapolation with the smallest β value removed is shown as a lighter gray band and a black triangle in cases where data were available at the smallest β value.

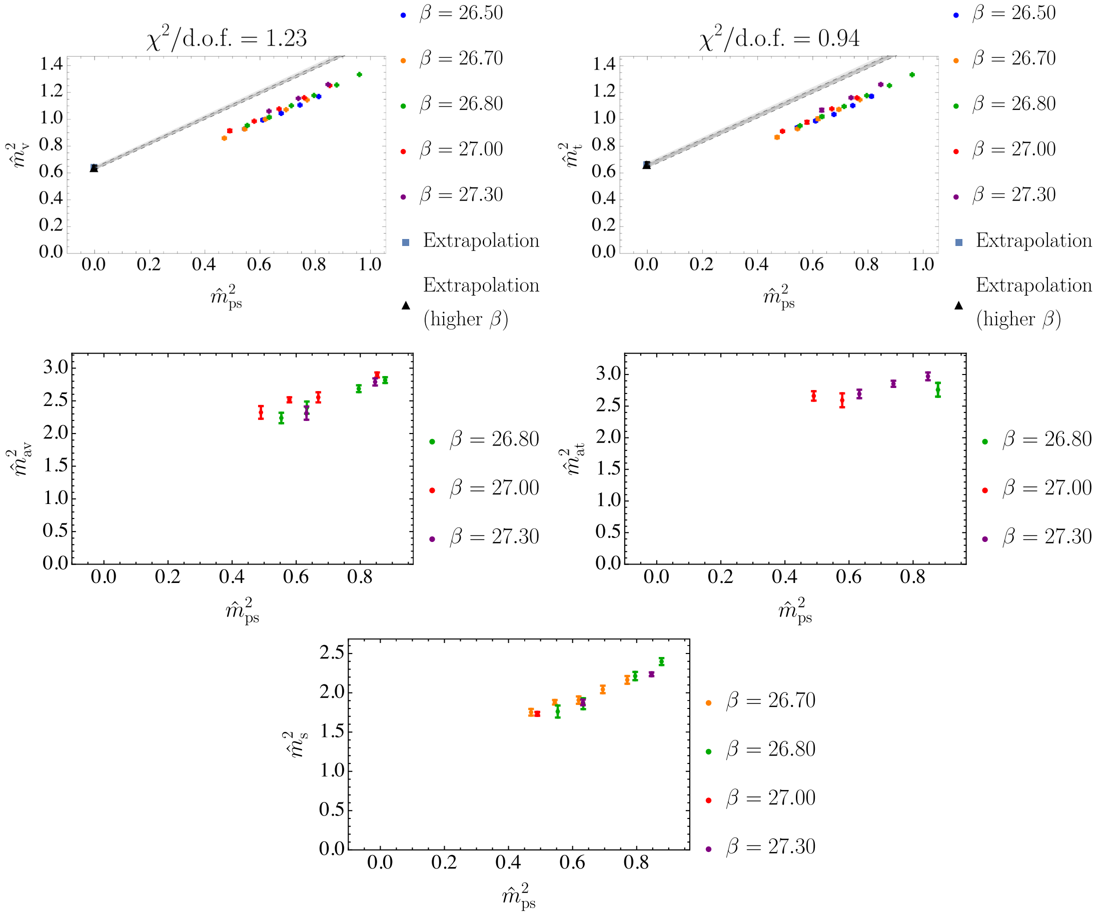

FIG. 21. Masses squared in the v, t, av, at, and s channels comprised of fermions in the antisymmetric representation of $Sp(8)$. The reduced chi-squared value is printed at the top of each plot. Data points in the pink shaded region are not included in the curve-fitting procedure. The gray band represents the continuum and massless extrapolation with the blue square being the observable and the vertical width corresponding to the statistical error. In instances where a reliable extrapolation cannot be made, no gray band is shown. All quantities are expressed in units of the gradient flow scale, w_0. The extrapolation with the smallest β value removed is shown as a lighter gray band and a black triangle in cases where data were available at the smallest β value.

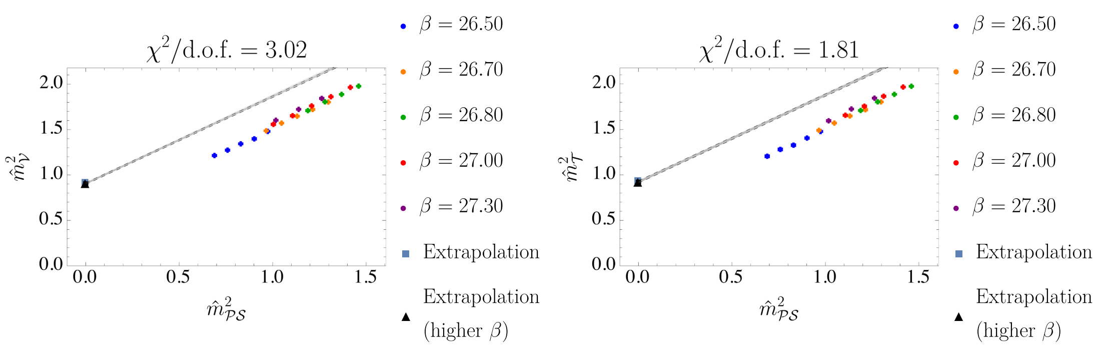

FIG. 22. Masses squared in the $\mathcal{V}$ and $\mathcal{T}$ channels comprised of fermions in the symmetric representation of $Sp(8)$. The reduced chi-squared value is printed at the top of each plot. Data points in the pink shaded region are not included in the curve-fitting procedure. The gray band represents the continuum and massless extrapolation with the blue square being the observable and the vertical width corresponding to the statistical error. In instances where a reliable extrapolation cannot be made, no gray band is shown. All quantities are expressed in units of the gradient flow scale, w_0. The extrapolation with the smallest β value removed is shown as a lighter gray band and a black triangle in cases where data were available at the smallest β value.

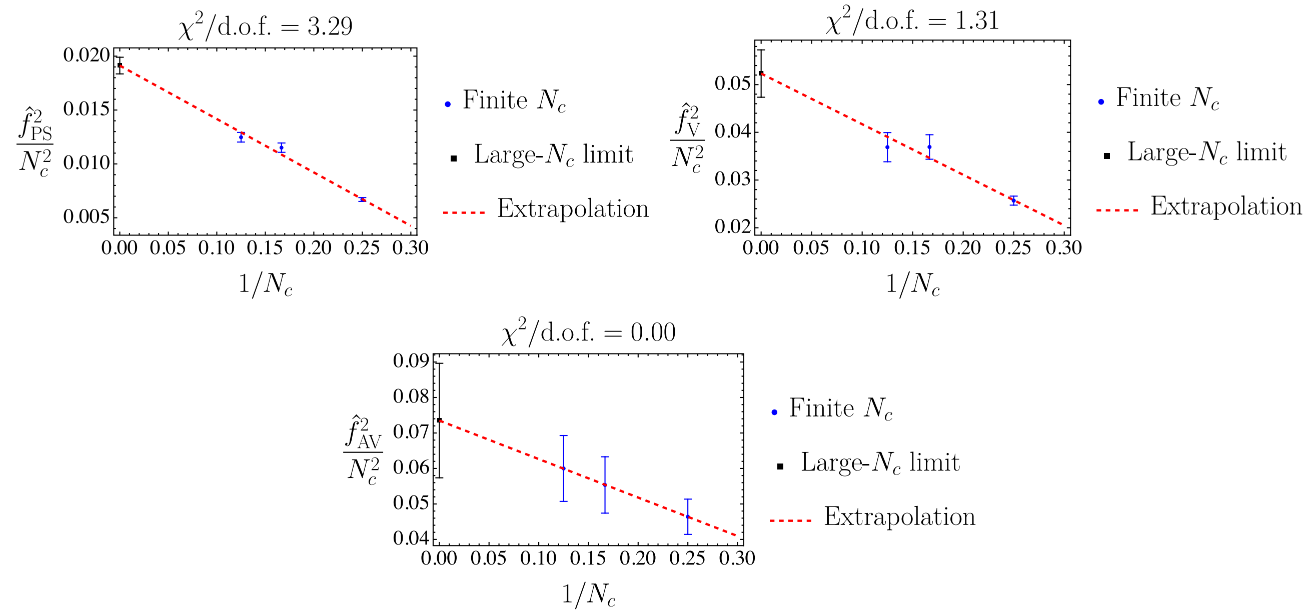

FIG. 23. Decay constants in PS, V and AV channels, with fermions in the fundamental representation extrapolated to $N_c \to \infty$. Reduced chi-squared values are printed at the top of each plot. All quantities are expressed in units of the gradient flow scale, w_0.

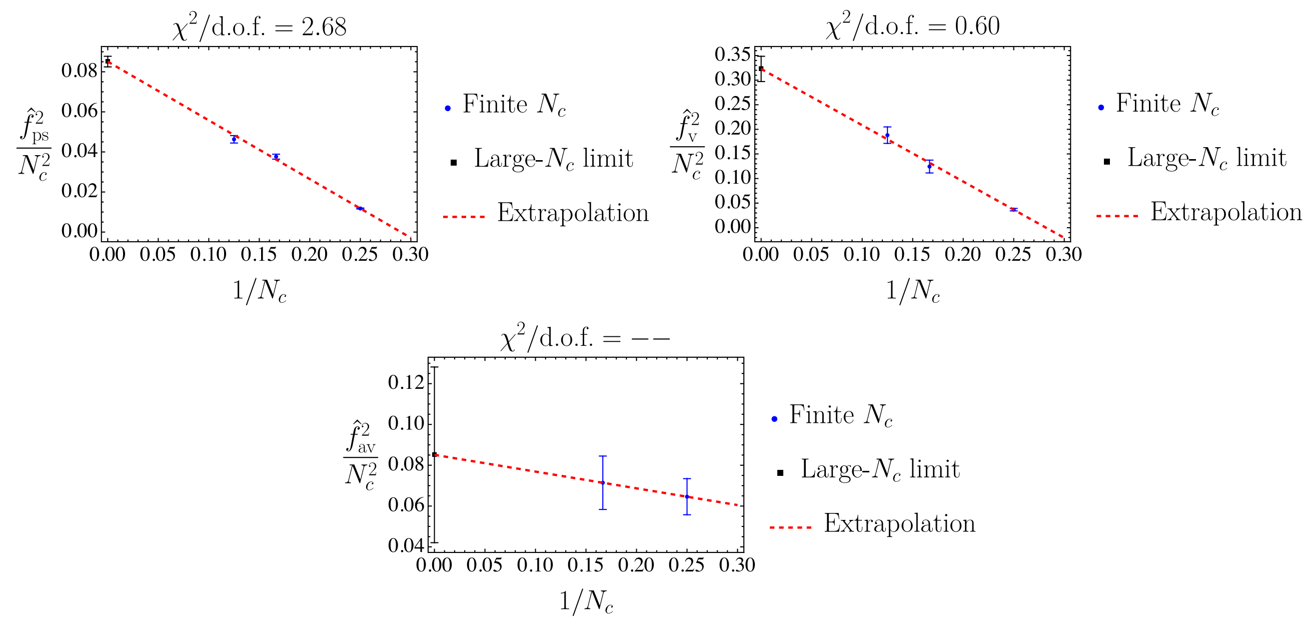

FIG. 24. Decay constants in ps, v, and av channels, with fermions in the antisymmetric representation extrapolated to $N_c \to \infty$. Reduced chi-squared values are printed at the top of each plot. All quantities are expressed in units of the gradient flow scale, w_0.

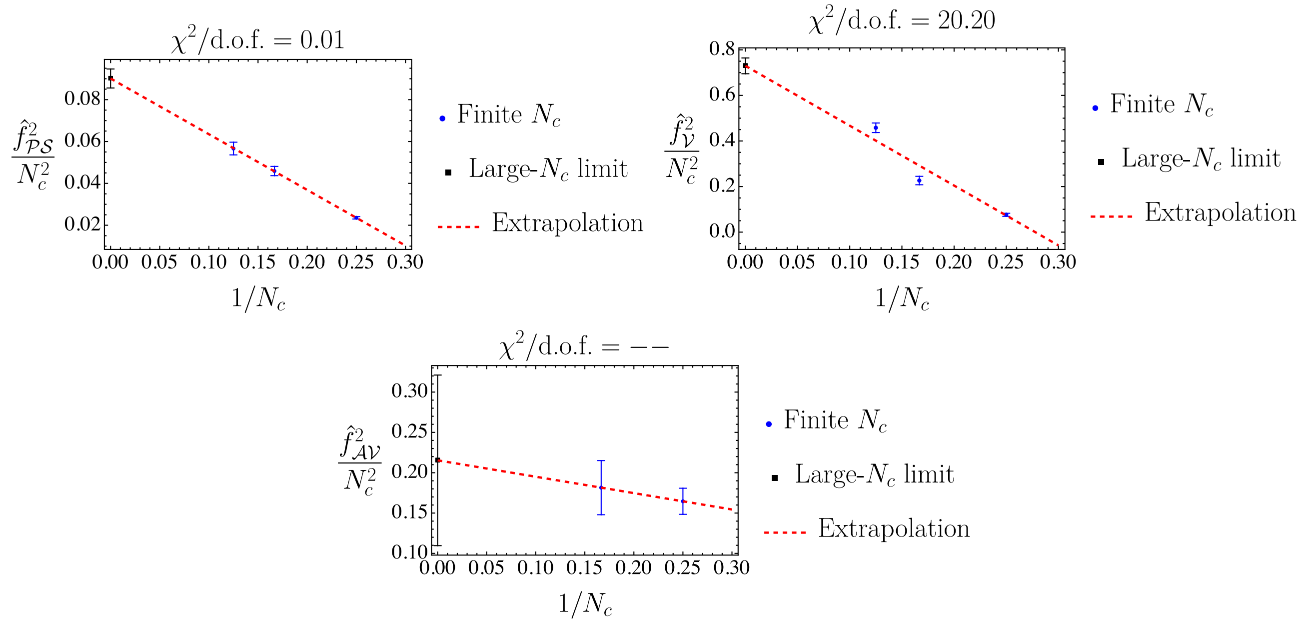

FIG. 25. Decay constants in $\mathcal{PS}$, $\mathcal{V}$, and $\mathcal{AV}$ channels, with fermions in the symmetric representation extrapolated to $N_c \to \infty$. Reduced chi-squared values are printed at the top of each plot. All quantities are expressed in units of the gradient flow scale, w_0.

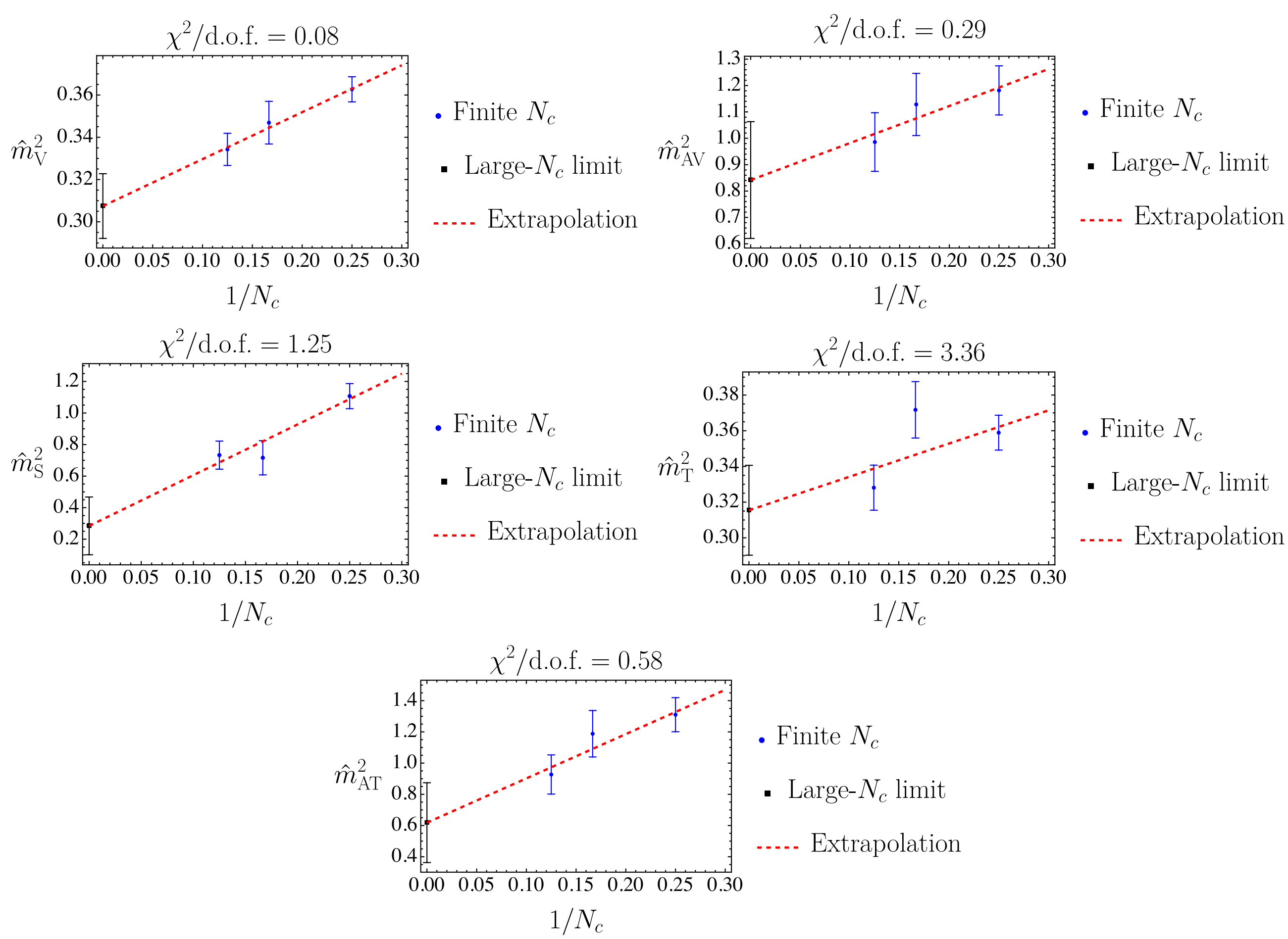

FIG. 26. Masses in V, T, AV, AT, and S channels, with fermions in the fundamental representation extrapolated to $N_c \to \infty$. Reduced chi-squared values are printed at the top of each plot. All quantities are expressed in units of the gradient flow scale, w_0.

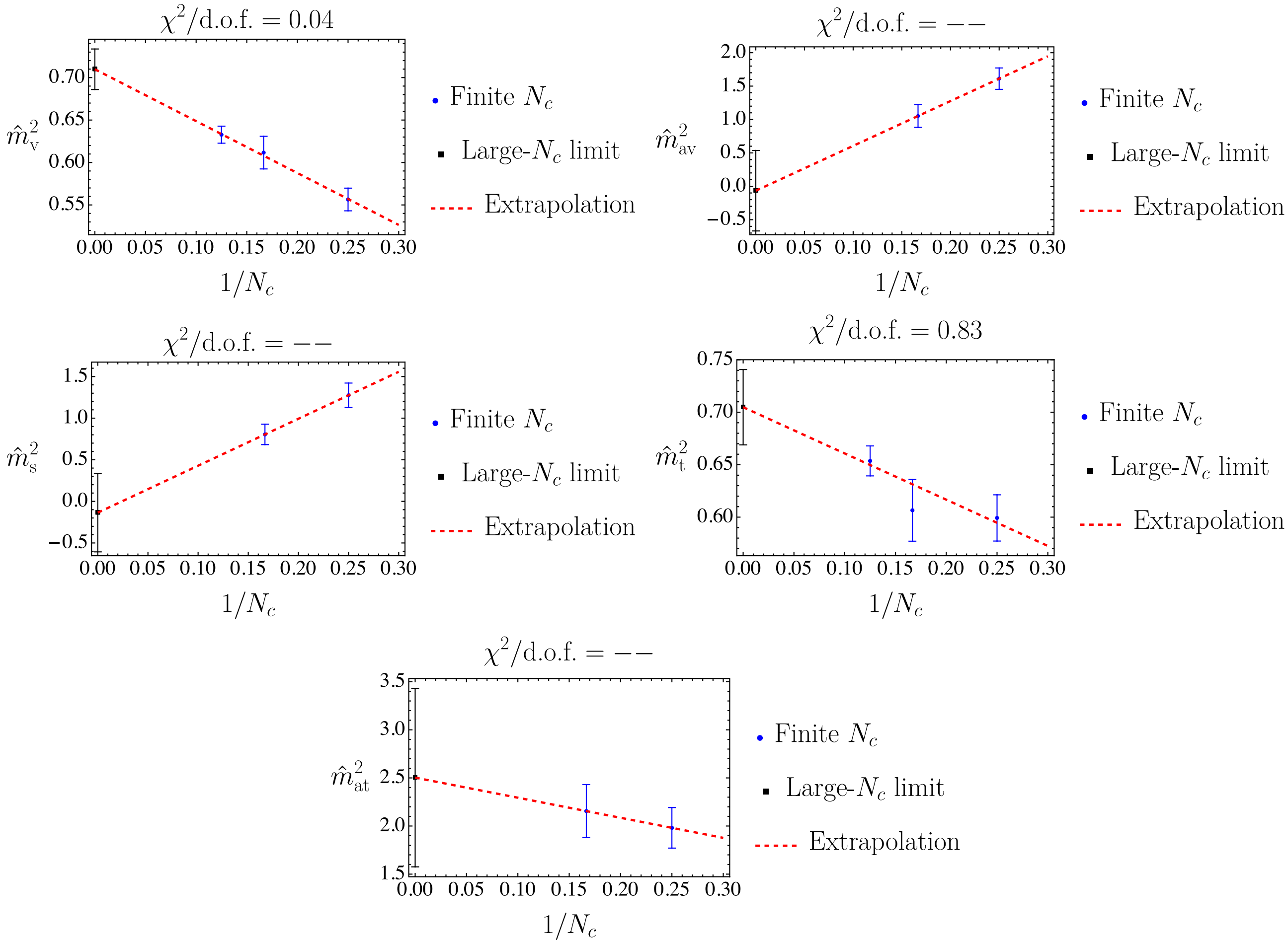

FIG. 27. Masses in v, t, av, at, and s channels, with fermions in the antisymmetric representation extrapolated to $N_c \to \infty$. Reduced chi-squared values are printed at the top of each plot. All quantities are expressed in units of the gradient flow scale, w_0.

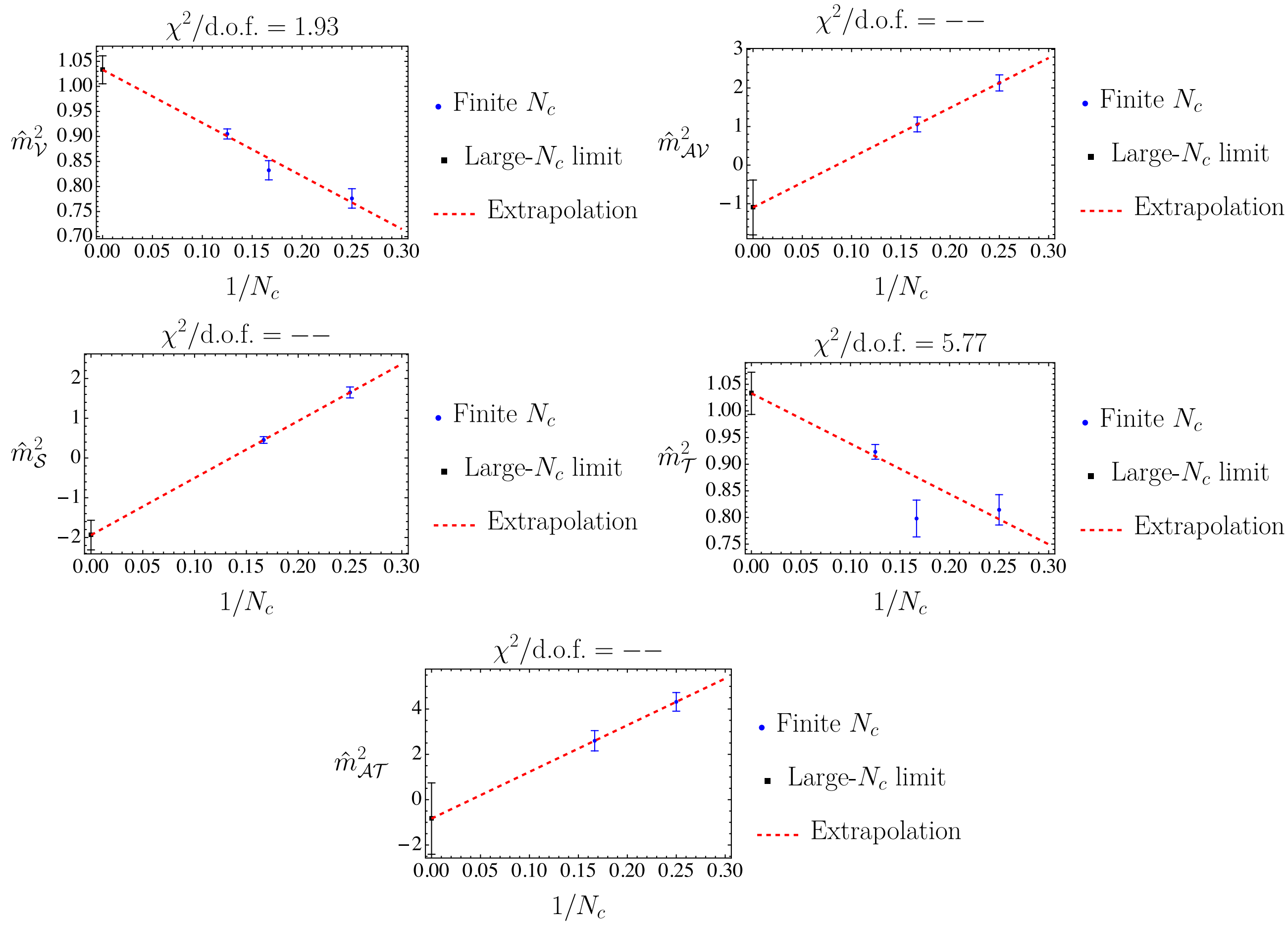

FIG. 28. Masses in $\mathcal{V}$, $\mathcal{T}$, $\mathcal{AV}$, $\mathcal{AT}$ and $\mathcal{S}$ channels, with fermions in the symmetric representation extrapolated to $N_c \to \infty$. Reduced chi-squared values are printed at the top of each plot. All quantities are expressed in units of the gradient flow scale, w_0.

[1] D. B. Kaplan and H. Georgi, SU(2) × U(1) breaking by vacuum misalignment, Phys. Lett. **136B**, 183 (1984).

[2] H. Georgi and D. B. Kaplan, Composite Higgs and custodial SU(2), Phys. Lett. **145B**, 216 (1984).

[3] M. J. Dugan, H. Georgi, and D. B. Kaplan, Anatomy of a composite Higgs model, Nucl. Phys. **B254**, 299 (1985).

[4] G. Panico and A. Wulzer, The composite Nambu-Goldstone Higgs, Lect. Notes Phys. **913**, 1 (2016) .

[5] O. Witzel, Review on composite Higgs models, Proc. Sci. LATTICE2018 (**2019**) 006.

[6] G. Cacciapaglia, C. Pica, and F. Sannino, Fundamental composite dynamics: A review, Phys. Rep. **877**, 1 (2020).

[7] G. Ferretti and D. Karateev, Fermionic UV completions of composite Higgs models, J. High Energy Phys. 03 (2014) 077.

[8] G. Ferretti, Gauge theories of partial compositeness: Scenarios for Run-II of the LHC, J. High Energy Phys. 06 (2016) 107.

[9] G. Cacciapaglia, G. Ferretti, T. Flacke, and H. Serôdio, Light scalars in composite Higgs models, Front. Phys. **7**, 22 (2019).

[10] E. Katz, A. E. Nelson, and D. G. E. Walker, The intermediate Higgs, J. High Energy Phys. 08 (2005) 074.

[11] R. Barbieri, B. Bellazzini, V. S. Rychkov, and A. Varagnolo, The Higgs boson from an extended symmetry, Phys. Rev. D **76**, 115008 (2007).

[12] P. Lodone, Vector-like quarks in a "composite" Higgs model, J. High Energy Phys. 12 (2008) 029.

[13] B. Gripaios, A. Pomarol, F. Riva, and J. Serra, Beyond the minimal composite Higgs model, J. High Energy Phys. 04 (2009) 070.

[14] J. Mrazek, A. Pomarol, R. Rattazzi, M. Redi, J. Serra, and A. Wulzer, The other natural two Higgs doublet model, Nucl. Phys. **B853**, 1 (2011).
[15] D. Marzocca, M. Serone, and J. Shu, General composite Higgs models, J. High Energy Phys. 08 (2012) 013.
[16] J. Barnard, T. Gherghetta, and T. S. Ray, UV descriptions of composite Higgs models without elementary scalars, J. High Energy Phys. 02 (2014) 002.
[17] C. Grojean, O. Matsedonskyi, and G. Panico, Light top partners and precision physics, J. High Energy Phys. 10 (2013) 160.
[18] G. Cacciapaglia and F. Sannino, Fundamental composite (Goldstone) Higgs dynamics, J. High Energy Phys. 04 (2014) 111.
[19] G. Ferretti, UV completions of partial compositeness: The case for a SU(4) gauge group, J. High Energy Phys. 06 (2014) 142.
[20] A. Arbey, G. Cacciapaglia, H. Cai, A. Deandrea, S. Le Corre, and F. Sannino, Fundamental composite electroweak dynamics: Status at the LHC, Phys. Rev. D **95**, 015028 (2017).
[21] G. Cacciapaglia, H. Cai, A. Deandrea, T. Flacke, S. J. Lee, and A. Parolini, Composite scalars at the LHC: The Higgs, the sextet and the octet, J. High Energy Phys. 11 (2015) 201.
[22] L. Vecchi, A dangerous irrelevant UV-completion of the composite Higgs, J. High Energy Phys. 02 (2017) 094.
[23] T. Ma and G. Cacciapaglia, Fundamental composite 2HDM: SU(N) with 4 flavours, J. High Energy Phys. 03 (2016) 211.
[24] F. Feruglio, B. Gavela, K. Kanshin, P. A. N. Machado, S. Rigolin, and S. Saa, The minimal linear sigma model for the Goldstone Higgs, J. High Energy Phys. 06 (2016) 038.
[25] T. DeGrand, M. Golterman, E. T. Neil, and Y. Shamir, One-loop chiral perturbation theory with two fermion representations, Phys. Rev. D **94**, 025020 (2016).
[26] S. Fichet, G. von Gersdorff, E. Pontón, and R. Rosenfeld, The excitation of the global symmetry-breaking vacuum in composite Higgs models, J. High Energy Phys. 09 (2016) 158.
[27] J. Galloway, A. L. Kagan, and A. Martin, A UV complete partially composite-pNGB Higgs, Phys. Rev. D **95**, 035038 (2017).
[28] A. Agugliaro, O. Antipin, D. Becciolini, S. De Curtis, and M. Redi, UV complete composite Higgs models, Phys. Rev. D **95**, 035019 (2017).
[29] A. Belyaev, G. Cacciapaglia, H. Cai, G. Ferretti, T. Flacke, A. Parolini, and H. Serodio, Di-boson signatures as standard candles for partial compositeness, J. High Energy Phys. 01 (2017) 094; 12 (2017) 088.
[30] C. Csaki, T. Ma, and J. Shu, Maximally symmetric composite Higgs models, Phys. Rev. Lett. **119**, 131803 (2017).
[31] M. Chala, G. Durieux, C. Grojean, L. de Lima, and O. Matsedonskyi, Minimally extended SILH, J. High Energy Phys. 06 (2017) 088.
[32] M. Golterman and Y. Shamir, Effective potential in ultraviolet completions for composite Higgs models, Phys. Rev. D **97**, 095005 (2018).
[33] C. Csáki, T. Ma, and J. Shu, Trigonometric parity for composite Higgs models, Phys. Rev. Lett. **121**, 231801 (2018).
[34] J. Serra and R. Torre, Neutral naturalness from the brother-Higgs model, Phys. Rev. D **97**, 035017 (2018).
[35] T. Alanne, D. Buarque Franzosi, and M. T. Frandsen, A partially composite Goldstone Higgs, Phys. Rev. D **96**, 095012 (2017).
[36] T. Alanne, D. Buarque Franzosi, M. T. Frandsen, M. L. A. Kristensen, A. Meroni, and M. Rosenlyst, Partially composite Higgs models: Phenomenology and RG analysis, J. High Energy Phys. 01 (2018) 051.
[37] F. Sannino, P. Stangl, D. M. Straub, and A. E. Thomsen, Flavor physics and flavor anomalies in minimal fundamental partial compositeness, Phys. Rev. D **97**, 115046 (2018).
[38] T. Alanne, N. Bizot, G. Cacciapaglia, and F. Sannino, Classification of NLO operators for composite Higgs models, Phys. Rev. D **97**, 075028 (2018).
[39] N. Bizot, G. Cacciapaglia, and T. Flacke, Common exotic decays of top partners, J. High Energy Phys. 06 (2018) 065.
[40] C. Cai, G. Cacciapaglia, and H.-H. Zhang, Vacuum alignment in a composite 2HDM, J. High Energy Phys. 01 (2019) 130.
[41] A. Agugliaro, G. Cacciapaglia, A. Deandrea, and S. De Curtis, Vacuum misalignment and pattern of scalar masses in the $SU(5)/SO(5)$ composite Higgs model, J. High Energy Phys. 02 (2019) 089.
[42] D. Buarque Franzosi, G. Cacciapaglia, and A. Deandrea, Sigma-assisted low scale composite Goldstone–Higgs, Eur. Phys. J. C **80**, 28 (2020).
[43] G. Cacciapaglia, T. Ma, S. Vatani, and Y. Wu, Towards a fundamental safe theory of composite Higgs and dark matter, Eur. Phys. J. C **80**, 1088 (2020).
[44] H. Gertov, A. E. Nelson, A. Perko, and D. G. E. Walker, Lattice-friendly gauge completion of a composite Higgs with top partners, J. High Energy Phys. 02 (2019) 181.
[45] V. Ayyar, M. F. Golterman, D. C. Hackett, W. Jay, E. T. Neil, Y. Shamir, and B. Svetitsky, Radiative contribution to the composite-Higgs potential in a two-representation lattice model, Phys. Rev. D **99**, 094504 (2019).
[46] G. Cacciapaglia, H. Cai, A. Deandrea, and A. Kushwaha, Composite Higgs and dark matter model in $SU(6)/SO(6)$, J. High Energy Phys. 10 (2019) 035.
[47] T. Appelquist, J. Ingoldby, and M. Piai, Nearly conformal composite Higgs model, Phys. Rev. Lett. **126**, 191804 (2021).
[48] D. Buarque Franzosi and G. Ferretti, Anomalous dimensions of potential top-partners, SciPost Phys. **7**, 027 (2019).
[49] G. Cacciapaglia, S. Vatani, and C. Zhang, Composite Higgs meets Planck scale: Partial compositeness from partial unification, Phys. Lett. B **815**, 136177 (2021).
[50] G. Cacciapaglia, A. Deandrea, T. Flacke, and A. M. Iyer, Gluon-photon signatures for color octet at the LHC (and beyond), J. High Energy Phys. 05 (2020) 027.

[51] H. Cai and G. Cacciapaglia, Singlet dark matter in the SU(6)/SO(6) composite Higgs model, Phys. Rev. D **103**, 055002 (2021).

[52] Z.-Y. Dong, C.-S. Guan, T. Ma, J. Shu, and X. Xue, UV completed composite Higgs model with heavy composite partners, Phys. Rev. D **104**, 035013 (2021).

[53] G. Cacciapaglia, T. Flacke, M. Kunkel, and W. Porod, Phenomenology of unusual top partners in composite Higgs models, J. High Energy Phys. 02 (2022) 208.

[54] A. Banerjee, D. B. Franzosi, and G. Ferretti, Modelling vector-like quarks in partial compositeness framework, J. High Energy Phys. 03 (2022) 200.

[55] T. Appelquist, J. Ingoldby, and M. Piai, Composite two-Higgs doublet model from dilaton effective field theory, Nucl. Phys. **B983**, 115930 (2022).

[56] R. Contino, Y. Nomura, and A. Pomarol, Higgs as a holographic pseudoGoldstone boson, Nucl. Phys. **B671**, 148 (2003).

[57] K. Agashe, R. Contino, and A. Pomarol, The minimal composite Higgs model, Nucl. Phys. **B719**, 165 (2005).

[58] K. Agashe and R. Contino, The minimal composite Higgs model and electroweak precision tests, Nucl. Phys. **B742**, 59 (2006).

[59] K. Agashe, R. Contino, L. Da Rold, and A. Pomarol, A custodial symmetry for $Zb\bar{b}$, Phys. Lett. B **641**, 62 (2006).

[60] R. Contino, L. Da Rold, and A. Pomarol, Light custodians in natural composite Higgs models, Phys. Rev. D **75**, 055014 (2007).

[61] A. Falkowski and M. Perez-Victoria, Electroweak breaking on a soft wall, J. High Energy Phys. 12 (2008) 107.

[62] R. Contino, The Higgs as a composite Nambu-Goldstone boson, in *Physics of the Large and the Small* (Word Scientific, Singapore, 2011), pp. 235–306.

[63] R. Contino, D. Marzocca, D. Pappadopulo, and R. Rattazzi, On the effect of resonances in composite Higgs phenomenology, J. High Energy Phys. 10 (2011) 081.

[64] F. Caracciolo, A. Parolini, and M. Serone, UV completions of composite Higgs models with partial compositeness, J. High Energy Phys. 02 (2013) 066.

[65] J. Erdmenger, N. Evans, W. Porod, and K. S. Rigatos, Gauge/gravity dynamics for composite Higgs models and the top mass, Phys. Rev. Lett. **126**, 071602 (2021).

[66] J. Erdmenger, N. Evans, W. Porod, and K. S. Rigatos, Gauge/gravity dual dynamics for the strongly coupled sector of composite Higgs models, J. High Energy Phys. 02 (2021) 058.

[67] D. Elander, M. Frigerio, M. Knecht, and J.-L. Kneur, Holographic models of composite Higgs in the Veneziano limit. Part I. Bosonic sector, J. High Energy Phys. 03 (2021) 182.

[68] D. Elander, M. Frigerio, M. Knecht, and J.-L. Kneur, Holographic models of composite Higgs in the Veneziano limit. Part II. Fermionic sector, J. High Energy Phys. 05 (2022) 066.

[69] D. Elander and M. Piai, Towards top-down holographic composite Higgs: Minimal coset from maximal supergravity, J. High Energy Phys. 03 (2022) 049.

[70] D. Elander, A. Fatemiabhari, and M. Piai, Toward minimal composite Higgs models from regular geometries in bottom-up holography, Phys. Rev. D **107**, 115021 (2023).

[71] J. Erdmenger, N. Evans, Y. Liu, and W. Porod, Holographic non-Abelian flavour symmetry breaking, Universe **9**, 289 (2023).

[72] D. B. Kaplan, Flavor at SSC energies: A New mechanism for dynamically generated fermion masses, Nucl. Phys. **B365**, 259 (1991).

[73] Y. Grossman and M. Neubert, Neutrino masses and mixings in nonfactorizable geometry, Phys. Lett. B **474**, 361 (2000).

[74] T. Gherghetta and A. Pomarol, Bulk fields and supersymmetry in a slice of AdS, Nucl. Phys. **B586**, 141 (2000).

[75] Z. Chacko and R. K. Mishra, Effective theory of a light dilaton, Phys. Rev. D **87**, 115006 (2013).

[76] Y. Hochberg, E. Kuflik, T. Volansky, and J. G. Wacker, Mechanism for thermal relic dark matter of strongly interacting massive particles, Phys. Rev. Lett. **113**, 171301 (2014).

[77] Y. Hochberg, E. Kuflik, H. Murayama, T. Volansky, and J. G. Wacker, Model for thermal relic dark matter of strongly interacting massive particles, Phys. Rev. Lett. **115**, 021301 (2015).

[78] Y. Hochberg, E. Kuflik, and H. Murayama, SIMP spectroscopy, J. High Energy Phys. 05 (2016) 090.

[79] M. Hansen, K. Langæble, and F. Sannino, SIMP model at NNLO in chiral perturbation theory, Phys. Rev. D **92**, 075036 (2015).

[80] N. Bernal and X. Chu, $\mathbb{Z}_2$ SIMP dark matter, J. Cosmol. Astropart. Phys. 01 (2016) 006.

[81] N. Bernal, X. Chu, and J. Pradler, Simply split strongly interacting massive particles, Phys. Rev. D **95**, 115023 (2017).

[82] A. Berlin, N. Blinov, S. Gori, P. Schuster, and N. Toro, Cosmology and accelerator tests of strongly interacting dark matter, Phys. Rev. D **97**, 055033 (2018).

[83] N. Bernal, X. Chu, S. Kulkarni, and J. Pradler, Self-interacting dark matter without prejudice, Phys. Rev. D **101**, 055044 (2020).

[84] Y.-D. Tsai, R. McGehee, and H. Murayama, Resonant self-interacting dark matter from dark QCD, Phys. Rev. Lett. **128**, 172001 (2022).

[85] D. Kondo, R. McGehee, T. Melia, and H. Murayama, Linear sigma dark matter, J. High Energy Phys. 09 (2022) 041.

[86] E. Witten, Cosmic separation of phases, Phys. Rev. D **30**, 272 (1984).

[87] M. Kamionkowski, A. Kosowsky, and M. S. Turner, Gravitational radiation from first order phase transitions, Phys. Rev. D **49**, 2837 (1994).

[88] B. Allen, The stochastic gravity wave background: Sources and detectionX, in *Proceedings, Les Houches School of Physics: Astrophysical Sources of Gravitational Radiation*, edited by J.-A. Marck and J.-P. Lasota, Cambridge Contemporary Astrophysics (1997), pp. 373–417, arXiv:gr-qc/9604033.

[89] P. Schwaller, Gravitational waves from a dark phase transition, Phys. Rev. Lett. **115**, 181101 (2015).

[90] D. Croon, V. Sanz, and G. White, Model discrimination in gravitational wave spectra from dark phase transitions, J. High Energy Phys. 08 (2018) 203.
[91] N. Christensen, Stochastic gravitational wave backgrounds, Rep. Prog. Phys. **82**, 016903 (2019).
[92] W.-C. Huang, M. Reichert, F. Sannino, and Z.-W. Wang, Testing the dark SU(N) Yang-Mills theory confined landscape: From the lattice to gravitational waves, Phys. Rev. D **104**, 035005 (2021).
[93] J. Halverson, C. Long, A. Maiti, B. Nelson, and G. Salinas, Gravitational waves from dark Yang-Mills sectors, J. High Energy Phys. 05 (2021) 154.
[94] Z. Kang, J. Zhu, and S. Matsuzaki, Dark confinement-deconfinement phase transition: A roadmap from Polyakov loop models to gravitational waves, J. High Energy Phys. 09 (2021) 060.
[95] M. Reichert, F. Sannino, Z.-W. Wang, and C. Zhang, Dark confinement and chiral phase transitions: Gravitational waves vs matter representations, J. High Energy Phys. 01 (2022) 003.
[96] M. Reichert and Z.-W. Wang, Gravitational waves from dark composite dynamics, EPJ Web Conf. **274**, 08003 (2022).
[97] R. Pasechnik, M. Reichert, F. Sannino, and Z.-W. Wang, Gravitational waves from composite dark sectors, J. High Energy Phys. 02 (2024) 159.
[98] N. Seto, S. Kawamura, and T. Nakamura, Possibility of direct measurement of the acceleration of the universe using 0.1-Hz band laser interferometer gravitational wave antenna in space, Phys. Rev. Lett. **87**, 221103 (2001).
[99] S. Kawamura *et al.*, The Japanese space gravitational wave antenna DECIGO, Classical Quantum Gravity **23**, S125 (2006).
[100] J. Crowder and N. J. Cornish, Beyond LISA: Exploring future gravitational wave missions, Phys. Rev. D **72**, 083005 (2005).
[101] V. Corbin and N. J. Cornish, Detecting the cosmic gravitational wave background with the big bang observer, Classical Quantum Gravity **23**, 2435 (2006).
[102] G. M. Harry, P. Fritschel, D. A. Shaddock, W. Folkner, and E. S. Phinney, Laser interferometry for the big bang observer, Classical Quantum Gravity **23**, 4887 (2006); **23**, 7361(E) (2006).
[103] S. Hild *et al.*, Sensitivity studies for third-generation gravitational wave observatories, Classical Quantum Gravity **28**, 094013 (2011).
[104] K. Yagi and N. Seto, Detector configuration of DECIGO/BBO and identification of cosmological neutron-star binaries, Phys. Rev. D **83**, 044011 (2011); **95**, 109901(E) (2017).
[105] B. Sathyaprakash *et al.*, Scientific objectives of Einstein Telescope, Classical Quantum Gravity **29**, 124013 (2012); **30**, 079501(E) (2013).
[106] E. Thrane and J. D. Romano, Sensitivity curves for searches for gravitational-wave backgrounds, Phys. Rev. D **88**, 124032 (2013).
[107] C. Caprini *et al.*, Science with the space-based interferometer eLISA. II: Gravitational waves from cosmological phase transitions, J. Cosmol. Astropart. Phys. 04 (2016) 001.
[108] P. Amaro-Seoane *et al.* (LISA Collaboration), Laser interferometer space antenna, arXiv:1702.00786.
[109] B. P. Abbott *et al.* (LIGO Scientific Collaboration), Exploring the sensitivity of next generation gravitational wave detectors, Classical Quantum Gravity **34**, 044001 (2017).
[110] S. Isoyama, H. Nakano, and T. Nakamura, Multiband gravitational-wave astronomy: Observing binary inspirals with a decihertz detector, B-DECIGO, Prog. Theor. Exp. Phys. **2018**, 073E01 (2018).
[111] J. Baker *et al.*, The laser interferometer space antenna: Unveiling the millihertz gravitational wave sky, arXiv: 1907.06482.
[112] V. Brdar, A. J. Helmboldt, and J. Kubo, Gravitational waves from first-order phase transitions: LIGO as a window to unexplored seesaw scales, J. Cosmol. Astropart. Phys. 02 (2019) 021.
[113] D. Reitze *et al.*, Cosmic Explorer: The U.S. contribution to gravitational-wave astronomy beyond LIGO, Bull. Am. Astron. Soc. **51**, 035 (2019).
[114] C. Caprini *et al.*, Detecting gravitational waves from cosmological phase transitions with LISA: An update, J. Cosmol. Astropart. Phys. 03 (2020) 024.
[115] M. Maggiore *et al.*, Science case for the Einstein Telescope, J. Cosmol. Astropart. Phys. 03 (2020) 050.
[116] K. Holland, M. Pepe, and U. J. Wiese, The deconfinement phase transition of Sp(2) and Sp(3) Yang-Mills theories in $(2+1)$-dimensions and $(3+1)$-dimensions, Nucl. Phys. **B694**, 35 (2004).
[117] G. Aad *et al.* (ATLAS Collaboration), Observation of a new particle in the search for the Standard Model Higgs boson with the ATLAS detector at the LHC, Phys. Lett. B **716**, 1 (2012).
[118] S. Chatrchyan *et al.* (CMS Collaboration), Observation of a new boson at a mass of 125 GeV with the CMS experiment at the LHC, Phys. Lett. B **716**, 30 (2012).
[119] E. Bennett, D. K. Hong, J.-W. Lee, C. J. D. Lin, B. Lucini, M. Piai, and D. Vadacchino, Sp(4) gauge theory on the lattice: Towards SU(4)/Sp(4) composite Higgs (and beyond), J. High Energy Phys. 03 (2018) 185.
[120] J.-W. Lee, E. Bennett, D. K. Hong, C. J. D. Lin, B. Lucini, M. Piai, and D. Vadacchino, Progress in the lattice simulations of Sp($2N$) gauge theories, Proc. Sci. LATTICE2018 (**2018**) 192.
[121] E. Bennett, D. K. Hong, J.-W. Lee, C. J. D. Lin, B. Lucini, M. Piai, and D. Vadacchino, Sp(4) gauge theories on the lattice: $N_f = 2$ dynamical fundamental fermions, J. High Energy Phys. 12 (2019) 053.
[122] E. Bennett, D. K. Hong, J.-W. Lee, C.-J. D. Lin, B. Lucini, M. Mesiti, M. Piai, J. Rantaharju, and D. Vadacchino, $Sp(4)$ gauge theories on the lattice: Quenched fundamental and antisymmetric fermions, Phys. Rev. D **101**, 074516 (2020).
[123] E. Bennett, J. Holligan, D. K. Hong, J.-W. Lee, C. J. D. Lin, B. Lucini, M. Piai, and D. Vadacchino, Color dependence of tensor and scalar glueball masses in Yang-Mills theories, Phys. Rev. D **102**, 011501 (2020).
[124] E. Bennett, J. Holligan, D. K. Hong, J.-W. Lee, C. J. D. Lin, B. Lucini, M. Piai, and D. Vadacchino, Glueballs and

strings in $Sp(2N)$ Yang-Mills theories, Phys. Rev. D **103**, 054509 (2021).

[125] B. Lucini, E. Bennett, J. Holligan, D. K. Hong, H. Hsiao, J.-W. Lee, C. J. D. Lin, M. Mesiti, M. Piai, and D. Vadacchino, Sp(4) gauge theories and beyond the standard model physics, EPJ Web Conf. **258**, 08003 (2022).

[126] E. Bennett, J. Holligan, D. K. Hong, H. Hsiao, J.-W. Lee, C. J. D. Lin, B. Lucini, M. Mesiti, M. Piai, and D. Vadacchino, Progress in $Sp(2N)$ lattice gauge theories, Proc. Sci. LATTICE2021 (**2022**) 308.

[127] E. Bennett, D. K. Hong, H. Hsiao, J.-W. Lee, C. J. D. Lin, B. Lucini, M. Mesiti, M. Piai, and D. Vadacchino, Lattice studies of the $Sp(4)$ gauge theory with two fundamental and three antisymmetric Dirac fermions, arXiv:2202.05516.

[128] E. Bennett, D. K. Hong, J.-W. Lee, C. J. D. Lin, B. Lucini, M. Piai, and D. Vadacchino, Color dependence of the topological susceptibility in Yang-Mills theories, Phys. Lett. B **835**, 137504 (2022).

[129] E. Bennett, D. K. Hong, J.-W. Lee, C. J. D. Lin, B. Lucini, M. Piai, and D. Vadacchino, Sp(2N) Yang-Mills theories on the lattice: Scale setting and topology, Phys. Rev. D **106**, 094503 (2022).

[130] J.-W. Lee, E. Bennett, D. K. Hong, H. Hsiao, C. J. D. Lin, B. Lucini, M. Piai, and D. Vadacchino, Spectroscopy of $Sp(4)$ lattice gauge theory with $n_f = 3$ antisymmetric fermions, Proc. Sci. LATTICE2022 (**2023**) 214.

[131] H. Hsiao, Ed Bennett, D. K. Hong, J.-W. Lee, C. J. D. Lin, B. Lucini, M. Piai, and D. Vadacchino, Spectroscopy of chimera baryons in a $Sp(4)$ lattice gauge theory, arXiv:2211.03955.

[132] A. Maas and F. Zierler, Strong isospin breaking in $\boldsymbol{Sp}(4)$ gauge theory, Proc. Sci. LATTICE2021 (**2022**) 130.

[133] F. Zierler and A. Maas, $Sp(4)$ SIMP dark matter on the lattice, Proc. Sci. LHCP2021 (**2021**) 162.

[134] S. Kulkarni, A. Maas, S. Mee, M. Nikolic, J. Pradler, and F. Zierler, Low-energy effective description of dark $Sp(4)$ theories, SciPost Phys. **14**, 044 (2023).

[135] E. Bennett, J. Holligan, D. K. Hong, H. Hsiao, J.-W. Lee, C. J. D. Lin, B. Lucini, M. Mesiti, M. Piai, and D. Vadacchino, Sp(2N) lattice gauge theories and extensions of the Standard Model of particle physics, Universe **9**, 236 (2023).

[136] E. Bennett, H. Hsiao, J.-W. Lee, B. Lucini, A. Maas, M. Piai, and F. Zierler, Singlets in gauge theories with fundamental matter, arXiv:2304.07191.

[137] E. Bennett *et al.*, Symplectic lattice gauge theories on grid: Approaching the conformal window, arXiv:2306.11649.

[138] D. Mason, B. Lucini, M. Piai, E. Rinaldi, and D. Vadacchino, The deconfinement phase transition in $Sp(2N)$ gauge theories and the density of states method, in *Proceedings of the 40th International Symposium on Lattice Field Theory* (2023), arXiv:2310.02145.

[139] N. Forzano *et al.*, Lattice studies of Sp(2N) gauge theories using GRID, in *Proceedings of the 40th International Symposium on Lattice Field Theory* (2023), arXiv:2310.02111.

[140] A. Hietanen, R. Lewis, C. Pica, and F. Sannino, Fundamental composite higgs dynamics on the lattice: SU(2) with two flavors, J. High Energy Phys. 07 (2014) 116.

[141] W. Detmold, M. McCullough, and A. Pochinsky, Dark nuclei. II. Nuclear spectroscopy in two-color QCD, Phys. Rev. D **90**, 114506 (2014).

[142] R. Arthur, V. Drach, M. Hansen, A. Hietanen, C. Pica, and F. Sannino, SU(2) gauge theory with two fundamental flavors: A minimal template for model building, Phys. Rev. D **94**, 094507 (2016).

[143] R. Arthur, V. Drach, A. Hietanen, C. Pica, and F. Sannino, $SU(2)$ gauge theory with two fundamental flavours: Scalar and pseudoscalar apectrum, arXiv:1607.06654.

[144] C. Pica, V. Drach, M. Hansen, and F. Sannino, Composite Higgs dynamics on the lattice, EPJ Web Conf. **137**, 10005 (2017).

[145] J.-W. Lee, B. Lucini, and M. Piai, Symmetry restoration at high-temperature in two-color and two-flavor lattice gauge theories, J. High Energy Phys. 04 (2017) 036.

[146] V. Drach, T. Janowski, and C. Pica, Update on SU(2) gauge theory with $N_F = 2$ fundamental flavours, EPJ Web Conf. **175**, 08020 (2018).

[147] V. Drach, T. Janowski, C. Pica, and S. Prelovsek, Scattering of Goldstone bosons and resonance production in a composite Higgs model on the lattice, J. High Energy Phys. 04 (2021) 117.

[148] V. Drach, P. Fritzsch, A. Rago, and F. Romero-López, Singlet channel scattering in a composite Higgs model on the lattice, Eur. Phys. J. C **82**, 47 (2022).

[149] V. Ayyar, T. DeGrand, M. Golterman, D. C. Hackett, W. I. Jay, E. T. Neil, Y. Shamir, and B. Svetitsky, Spectroscopy of SU(4) composite Higgs theory with two distinct fermion representations, Phys. Rev. D **97**, 074505 (2018).

[150] V. Ayyar, T. Degrand, D. C. Hackett, W. I. Jay, E. T. Neil, Y. Shamir, and B. Svetitsky, Baryon spectrum of SU(4) composite Higgs theory with two distinct fermion representations, Phys. Rev. D **97**, 114505 (2018).

[151] V. Ayyar, T. DeGrand, D. C. Hackett, W. I. Jay, E. T. Neil, Y. Shamir, and B. Svetitsky, Finite-temperature phase structure of SU(4) gauge theory with multiple fermion representations, Phys. Rev. D **97**, 114502 (2018).

[152] V. Ayyar, T. DeGrand, D. C. Hackett, W. I. Jay, E. T. Neil, Y. Shamir, and B. Svetitsky, Partial compositeness and baryon matrix elements on the lattice, Phys. Rev. D **99**, 094502 (2019).

[153] G. Cossu, L. Del Debbio, M. Panero, and D. Preti, Strong dynamics with matter in multiple representations: SU(4) gauge theory with fundamental and sextet fermions, Eur. Phys. J. C **79**, 638 (2019).

[154] A. Lupo, M. Panero, N. Tantalo, and L. Del Debbio, Spectral reconstruction in SU(4) gauge theory with fermions in multiple representations, Proc. Sci. LATTICE2021 (**2022**) 092.

[155] A. Hasenfratz, E. T. Neil, Y. Shamir, B. Svetitsky, and O. Witzel, Infrared fixed point and anomalous dimensions in a composite Higgs model, arXiv:2304.11729.

[156] Y. Aoki *et al.* (LatKMI Collaboration), Light composite scalar in eight-flavor QCD on the lattice, Phys. Rev. D **89**, 111502 (2014).

[157] T. Appelquist *et al.*, Strongly interacting dynamics and the search for new physics at the LHC, Phys. Rev. D **93**, 114514 (2016).

[158] Y. Aoki *et al.* (LatKMI Collaboration), Light flavor-singlet scalars and walking signals in $N_f = 8$ QCD on the lattice, Phys. Rev. D **96**, 014508 (2017).
[159] A. D. Gasbarro and G. T. Fleming, Examining the low energy dynamics of walking gauge theory, Proc. Sci. LATTICE2016 (**2017**) 242.
[160] T. Appelquist *et al.* (Lattice Strong Dynamics Collaboration), Nonperturbative investigations of SU(3) gauge theory with eight dynamical flavors, Phys. Rev. D **99**, 014509 (2019).
[161] T. Appelquist *et al.* (Lattice Strong Dynamics (LSD) Collaboration), Goldstone boson scattering with a light composite scalar, Phys. Rev. D **105**, 034505 (2022).
[162] A. Hasenfratz, Emergent strongly coupled ultraviolet fixed point in four dimensions with eight Kähler-Dirac fermions, Phys. Rev. D **106**, 014513 (2022).
[163] T. Appelquist *et al.* (Lattice Strong Dynamics (LSD) Collaboration), Hidden conformal symmetry from the lattice, arXiv:2305.03665.
[164] R. C. Brower *et al.* (Lattice Strong Dynamics Collaboration), Light scalar meson and decay constant in SU(3) gauge theory with eight dynamical flavors, arXiv:2306.06095.
[165] J. M. Maldacena, The large N limit of superconformal field theories and supergravity, Adv. Theor. Math. Phys. **2**, 231 (1998).
[166] S. S. Gubser, I. R. Klebanov, and A. M. Polyakov, Gauge theory correlators from noncritical string theory, Phys. Lett. B **428**, 105 (1998).
[167] E. Witten, Anti-de Sitter space and holography, Adv. Theor. Math. Phys. **2**, 253 (1998).
[168] O. Aharony, S. S. Gubser, J. M. Maldacena, H. Ooguri, and Y. Oz, Large N field theories, string theory and gravity, Phys. Rep. **323**, 183 (2000).
[169] B. Lucini and M. Panero, SU(N) gauge theories at large N, Phys. Rep. **526**, 93 (2013).
[170] M. García Pérez, Prospects for large N gauge theories on the lattice, Proc. Sci. LATTICE2019 (**2020**) 276.
[171] P. Hernández and F. Romero-López, The large N_c limit of QCD on the lattice, Eur. Phys. J. A **57**, 52 (2021).
[172] T. A. DeGrand and E. Wickenden, Lattice study of the chiral properties of large N_c QCD, arXiv:2309.12270.
[173] B. Sheikholeslami and R. Wohlert, Improved continuum limit lattice action for QCD with Wilson fermions, Nucl. Phys. **B259**, 572 (1985).
[174] G. Rupak and N. Shoresh, Chiral perturbation theory for the Wilson lattice action, Phys. Rev. D **66**, 054503 (2002).
[175] S. R. Sharpe and R. L. Singleton, Jr, Spontaneous flavor and parity breaking with Wilson fermions, Phys. Rev. D **58**, 074501 (1998).
[176] K. Symanzik, Continuum limit and improved action in lattice theories. 1. Principles and φ^4 theory, Nucl. Phys. **B226**, 187 (1983).
[177] M. Luscher, S. Sint, R. Sommer, and P. Weisz, Chiral symmetry and O(a) improvement in lattice QCD, Nucl. Phys. **B478**, 365 (1996).
[178] A. Kennedy and B. Pendleton, Improved heatbath method for Monte Carlo calculations in lattice gauge theories, Phys. Lett. **156B**, 393 (1985).
[179] C. Whitmer, Over-relaxation methods for Monte Carlo simulations of quadratic and multiquadratic actions, Phys. Rev. D **29**, 306 (1984).
[180] S. L. Adler, Over-relaxation method for the Monte Carlo evaluation of the partition function for multiquadratic actions, Phys. Rev. D **23**, 2901 (1981).
[181] M. Lüscher, Properties and uses of the Wilson flow in lattice QCD, J. High Energy Phys. 08 (2010) 071; 03 (2014) 092(E).
[182] M. Lüscher, Future applications of the Yang-Mills gradient flow in lattice QCD, Proc. Sci. LATTICE2013 (**2014**) 016.
[183] M. Luscher and P. Weisz, Perturbative analysis of the gradient flow in non-Abelian gauge theories, J. High Energy Phys. 02 (2011) 051.
[184] S. Borsányi, S. Dürr, Z. Fodor, C. Hoelbling, S. D. Katz, S. Krieg, T. Kurth, L. Lellouch, T. Lippert, and C. McNeile (BMW Collaboration), High-precision scale setting in lattice QCD, J. High Energy Phys. 09 (2012) 010.
[185] J. Holligan, E. Bennett, D. K. Hong, J.-W. Lee, C.-J. D. Lin, B. Lucini, M. Piai, and D. Vadacchino, On the spectrum of mesons in quenched Sp(2N) gauge theories—Data release, 10.5281/zenodo.10932404 (Zenodo, 2024).
[186] C. W. Bernard and M. F. L. Golterman, Finite volume two pion energies and scattering in the quenched approximation, Phys. Rev. D **53**, 476 (1996).
[187] C. J. D. Lin, G. Martinelli, E. Pallante, C. T. Sachrajda, and G. Villadoro, Finite volume two pion amplitudes in the I = 0 channel, Phys. Lett. B **553**, 229 (2003).
[188] J. Erlich, E. Katz, D. T. Son, and M. A. Stephanov, QCD and a holographic model of hadrons, Phys. Rev. Lett. **95**, 261602 (2005).
[189] S. Weinberg, Precise relations between the spectra of vector and axial vector mesons, Phys. Rev. Lett. **18**, 507 (1967).
[190] M. E. Peskin and T. Takeuchi, Estimation of oblique electroweak corrections, Phys. Rev. D **46**, 381 (1992).
[191] R. Barbieri, A. Pomarol, R. Rattazzi, and A. Strumia, Electroweak symmetry breaking after LEP-1 and LEP-2, Nucl. Phys. **B703**, 127 (2004).
[192] S. Eidelman *et al.* (Particle Data Group), Review of particle physics, Phys. Lett. B **592**, 1 (2004).
[193] E. Bennett, D. K. Hong, H. Hsiao, J.-W. Lee, C. J. D. Lin, B. Lucini, M. Piai, and D. Vadacchino, Lattice investigations of the chimera baryon spectrum in the Sp(4) gauge theory, arXiv:2311.14663.
[194] J. Holligan, E. Bennett, D. K. Hong, J.-W. Lee, C.-J. D. Lin, B. Lucini, M. Piai, and D. Vadacchino, On the spectrum of mesons in quenched Sp(2N) gauge theories—Analysis workflow, 10.5281/zenodo.10932408 (Zenodo, 2024).
[195] M. Luscher, K. Symanzik, and P. Weisz, Anomalies of the free loop wave equation in the WKB approximation, Nucl. Phys. **B173**, 365 (1980).